Differential Proteomic Analysis of DEN-Induced Hepatocellular Carcinoma in Male and Female Balb/c Mice Reveals Novel Gender Specific Markers

***Salmma Salamah Salihah[1], Muhammad Tahir[2], Bareera Bibi[3], Rabia Sultan[4], Martin R. Larsen[2], Munazza Raza Mirza[4], Sana Mahmood[1], Muhammad Rizwan Alam[5], *Asma Gul[1]**

[1] Department of Biological Sciences, International Islamic University Islamabad, Islamabad, Pakistan

[2] Biomedical Mass Spectrometry and Systems Biology, University of South Denmark, Odense, Denmark

[3] School of Interdisciplinary Engineering & Science (SINES), NUST, Islamabad, Pakistan

[4] Dr. Panjwani Center for Molecular Medicine and Drug Research, International Center for Chemical and Biological Sciences, University of Karachi, Karachi, Pakistan

[5] Cell Biology Laboratory, Department of Biochemistry, Quaid-i-Azam University, Islamabad 45320, Pakistan

***Corresponding Author:** Salmma Salamah Salihah and Asma Gul

Authors' Disclosures

The authors declare no potential conflicts of interest.

ABSTRACT

Hepatocellular carcinoma is one of the leading causes of death with a higher prevalence in males compared to females due to distinct progression and pathogenesis patterns in both genders. This study aimed at creating, characterizing, and proteome profiling, a DEN-induced HCC model of male and female Balb/c mice. Proteins were extracted from characterized mouse models and subjected to mass spectrometry and subsequent bioinformatics analysis. The results revealed that the differentially enriched signaling pathways in treated female mice mainly belonged to the constituent of cytoskeleton, and mitochondria, including metabolic and oxidoreductase activity clusters. The enriched signaling pathways in treated male mice were related to translation, ribosomal structural and binding subunits and mRNA binding, metabolic processes, glutathione transferase activity, oxidoreductase activity, and mitochondrial activity. Protein-protein interaction analysis revealed the top ten genes ranked by highest maximal clique centrality. Survival Analysis using UACLAN indicated that among the hub genes of DEN-treated female mice, only the upregulation of NDUFA8 was associated with patient survival. In DEN-treated male mice downregulation of EEF2 and upregulation of RPL7A, RPL18A, RPL27A, RPS3, RPS 11 and

SERBP1 was associated with poor survival. The study indicates that the protein families associated with poor survival, ribosomal and RNA binding proteins in males, and mitochondrial complex 1 proteins in females are novel gender-specific prognostic markers and therapeutic targets for HCC.

Key Words: Hepatocellular Carcinoma, Proteomics, DEN induced mouse model, Mass Spectrometry, Prognostic Biomarkers

Introduction

Hepatocellular carcinoma (HCC) accounts for 80-90% of liver cancer cases, making it the most common type of hepatic malignancy (Llovet et al., 2021). It poses a serious burden on global health and the economy, especially in Asia (Kulik & El-Serag, 2019). HCC has a low five-year survival rate of approximately 18%. It is the third leading cause of cancer-related deaths worldwide (Siegel et al., 2022) and the second leading cause in Asia (Kim, 2024). Liver cancer, including cholangiocarcinoma and HCC, has been ranked as the second major contributor to cancer-related loss of lives globally from 2005-2015, with an increase of 4.6% in absolute years of life lost (El-Serag, 2012; Tang et al., 2018). Approximately 80% of HCC cases are concentrated in Eastern Asia and Sub-Saharan Africa consistent with the higher incidences of chronic hepatitis B virus in these regions (Kim, 2024).

HCC is more prevalent in males compared to females, with a ratio of 4:1 (Park et al., 2015). Females are also associated with a better survival rate compared to their male counterparts with HCC (Lam et al., 2005). Despite the established etiological variation in chronic liver disease, the disparity in the prognosis and characteristics of HCC between genders remains poorly understood (Liou et al., 2023). Sex hormones, including androgens and estrogens, play roles in HCC risk and progression. (Ito and Nguyen, 2023).

Various animal models are used to study HCC, including gene editing, in-situ transplantation, and chemical induction (He et al., 2015). However, the first two methods are limited in their ability to capture only a specific aspect of the tumor, hence missing the broader clinical picture of tumor progression and immune dysregulation (Brown et al., 2018; Liu et al., 2022). Diethyl nitrosamine (DEN) is a potent liver carcinogen used to induce HCC by causing DNA ethylation, and genetic mutations, and ultimately leading to the transformation of normal hepatocytes into cancer cells following a single dose (Santos et al., 2017). DEN is activated by cytochrome P450, leading to the formation of DNA adducts and at the same time generation of reactive oxygen species (ROS) which cause DNA damage, oxidative stress, and eventually HCC (Memon et al., 2020). The DEN-induced mouse model closely replicates gene expression signatures of human poor prognosis HCC and hence showcases similar low β-catenin levels, high proliferation, chromosomal instability, ubiquitination, and apoptosis (Li et al., 2004; Kamino et al., 2011; Wang et al., 2012).

Due to the heterogeneous nature of HCC, the development of gender-specific animal models and their molecular characterization is of prime importance in preclinical studies. Although the proteomic profile of DEN and CCl_4-induced HCC in mouse models has been studied, the gender-dependent nature of HCC means that genomic, transcriptomic, and proteomic data for either gender alone does not suffice to represent the differential proteomic landscape. This creates an urgent need for comparative protein profiling of DEN-induced HCC in male and female mouse models.

In this study, a DEN-induced HCC model was used, characterized, and subjected to proteome profiling. The study provided significant proteomic data that helped in understanding the differential expression patterns of DEN-induced HCC at the protein level in Balb/c mice.

Materials and methods

Mouse model and tissue collection

Animals were obtained from the National Institute of Health, Islamabad, Pakistan. The protocol was approved by the Ethical Committee, of the International Islamic University Islamabad. The animals were treated in accordance with the guidelines of the ethical committee. A total of 20 Balb/c mice at four weeks of age(17g body weight) were maintained in constant 12 h light/dark cycles and temperature-controlled conditions (22-25°C). They were fed with a standard mouse diet and water ad libitum. Balb/c mice were divided into treatment and control groups. Each group was further comprised of five male and six female mice. The animals from the experimental group were intraperitoneally treated with DEN (Sigma-Aldrich, USA) (100mg/kg) at four weeks of age. Animals from the control group were treated with solvent (normal saline) at the same age. Both treatment and control groups were followed till 32 weeks. After the completion of the experimental period surviving mice were terminally anesthetized by an overdose of Sodium pentobarbital, and then sacrificed to harvest liver tissue from both treatment and control groups. The excised liver tissue was rinsed with PBS and macroscopically evaluated for lesions/nodules before dividing into two sections. One of the sections was fixed with 4% formaldehyde for histological analysis and immunohistochemical staining analysis while the other section was used for proteomic profiling.

H&E staining & immunohistostaining

Formaldehyde-fixed tissues were embedded in paraffin and sectioned. Liver tissue sections (5μm) from both tumor and non-tumor areas were mounted on glass slides and deparaffinized with three successive xylene treatments. Sections were hydrated through successive treatments with 100, 95, and 70% ethanol and stained with 100% Mayer's Hematoxylin-5 min and counterstained with Eosin. The sections were then dehydrated with

106 70, 95 and 100% ethanol respectively followed by Xylene treatments. Stained sections were
107 mounted using Permount and allowed to dry before microscopic examination.

108 For immunohistochemistry an antigen-retrieval method based on microwave
109 pretreatment and 0.01 M sodium citrate buffer (pH 6) was used as previously described
110 (Maffini et al., 2001). Antibodies, including anti Ki67 antibody (Cat # PA0118, Leica
111 biosystems), Vimentin (Cat # NCL-VIM-V9, Leica biosystems) and E-Cadherin (Cat# PA0387,
112 Leica biosystems) were used at 1:400, 1:1000, 1:1000-4000 dilutions, respectively. The
113 antigen- antibody reaction was visualized using the streptavidin-peroxidase complex, with
114 diaminobenzidine tetrahydrochloride (Sigma-Aldrich) as the chromogen. Counterstaining
115 was carried out with Harris' hematoxylin. Images were captured with an Olympus BX53
116 microscope equipped with Olympus digital camera.

117 **Sample preparation for proteome analysis**

118 Liver sections were rinsed with PBS and immersed in freshly supplemented RIPA
119 buffer (10 mM Tris-HCl, 140 mM NaCl, 0.1% SDS, 1% Triton X 100, and 0.01% Sodium
120 deoxycholate). The tissues were homogenized on ice for 20 minutes using a tissue
121 homogenizer. After centrifugation (13, 000× *g*; 20 min, 4 °C), supernatants were stored at -
122 80°C. Protein estimation was performed through Bradford Assay.

123 **Tryptic digestion**

124 For the enzymatic digestion of protein standard (α-casein, β-casein, and ovalbumin)
125 and protein samples, 0.1mg/mL(200µL) was aliquoted. To adjust the pH (~8) 1M NH4HCO3
126 (160µL) was added to the aliquots. Protein samples were reduced and denatured by adding
127 45 mM DTT and 40 mM nOGP. Afterward, the vials were incubated on a thermomixer
128 (Eppendorf, Germany) for 30 mins at 90°C and 800 rpm. Protein solutions were allowed to
129 cool at room temperature. Samples alkylation was carried out at room temperature by
130 adding 100 mM of iodoacetamide (IAA) and the vials were incubated in the dark for 15 mins.
131 Deionized water was added followed by the addition of 2µg trypsin. After adding trypsin
132 samples were digested on a thermomixer (Eppendorf, Germany) for 16 hours at 600 rpm and
133 37°C. The digestion process was stopped by adding 2% TFA (60µL, pH ≤3). All digests were
134 stored at -20°C.

135 **Mass spectrometry analysis**

136 Peptide digests were analyzed by nano- LC-MS/MS system on a Q Exactive HF
137 Orbitrap LC-MS/MS system (Thermo Fischer) coupled to an EASY-LC 1000 system (Thermo
138 Fischer Scientific). Long-fused silica capillary column (PicoFirt 18 cm, 75 m inner diameter)
139 was packed in-house with reversed-phase Repro-SilPur C18-AQ 3 m resin and used to load
140 1mg of purified peptides. Peptides were eluted from Buffer A (0.1% Formic acid) at a flow
141 rate of 250 nL/min followed by elusion through buffer B (95% acetonitrile in 0.1% Formic
142 acid). The gradient gradually increased in B from 5% to 28% in 40 mins, 45% in 60 mins, and

143 finally to 100% in the end. The Q-Exactive HF was set up to operate in data-dependent
144 acquisition mode with the following parameters: full scan automatic gain control (AGC)
145 target 3e6 at 120000 FWHM resolution, scan range 350-1600 mz, Orbitrap full scan
146 maximum injection time 100 ms, normalized collision energy 28, a dynamic exclusion time of
147 the 30s, an isolation window of 1.2 m/z and top 20 MS2 scans per MS full scan.

148 **Statistical data analysis**

149 The statistical analysis of the data was performed by importing protein groups from
150 MaxQuant. The analysis was carried out on Perseus v.1.6.10.50 after removing potential
151 contaminants, reverse database hits, and protein identified by site, log2 transformation was
152 carried out. The samples were categorized into four groups (DEN-treated female mice, DEN-
153 treated male mice, Vehicle-treated male mice, and vehicle-treated female mice). Proteins
154 were further filtered to include only those with at least three valid values in each group.
155 Significance testing of protein LFQ intensities was carried out by post hoc Tukey's HSD test
156 for one-way ANOVA with a p-value threshold of <0.05 (Benjamini-Hochberg FDR at 0.05)
157 considered significant. Groupwise comparisons were carried out using a functional analysis
158 tool. Principal component analysis was carried out to see the differentiation of treated and
159 control samples. Heat maps were generated using Perseus v.1.6.10.50, displaying protein
160 intensities with non-supervised hierarchical clustering of rows. Volcano plots were made to
161 represent differentially expressed proteins.

162 **Gene enrichment analysis**

163 The biological significance of the differentially expressed proteins was determined
164 through Gene Ontology (GO), Kyoto Encyclopedia of Genes and Genomes (KEGG)
165 enrichment analysis (https://www.kegg.jp/kegg/pathway.html, p adj value < 0.05),
166 Reactome analysis (https://reactome.org/Pathway.html, p adj value < 0.05) that identifies
167 pathways enriched in the proteins of interest and through Gene ontology enrichment
168 analysis to determine whether GO terms about specific processes, molecular functions, or
169 cellular components are represented within the DEP set. Overrepresentation analysis of GO,
170 KEGG, and Reactome terms was performed using the R package (clusterprofiler).

171 **PPI and hub proteins**

172 Functional associations or physical interactions between proteins network was
173 visualized using the STRING database and Cytoscape. The significant module for each
174 network was obtained by MCODE using default parameters. Moreover, the MCC method was
175 used to select hub genes from the PPI network using the CytoHubba plugin of Cytoscape.

176 **Survival analysis**

177 The clinical value of differentially expressed proteins was estimated by converting 20
178 hub proteins to their human homologs using the "biomaRt" R package. Protein expression of

179 human homologous proteins corresponding to DEPs was matched with overall survival using
180 the UALCAN tool.

181 **Results**

182 **DEN-Induced Mouse Model for Male and Female HCC**

183 DEN-induced HCC mouse model for male and female Balb/c mice was constructed
184 following one of the methods described by Peng et al. (2024) with some modifications.
185 Consistent with the gender bias in HCC all six female mice in the treatment group survived
186 until 8 months whereas only 2 male mice survived till the end. Subsequent analysis was
187 performed with the surviving individuals of the groups. Normal and tumor tissues with
188 internal and external controls were collected from control and treated mice of both genders
189 separately for the histological and proteomic analysis (**Fig. 1A**). In the DEN-induced mouse
190 model multiple tumors developed in the liver. H&E staining revealed that hepatocytes in the
191 liver of control mice were neatly arranged with normal cellular morphology. In contrast,
192 hepatocytes in the tumor tissue showed disorganized morphology, large nuclei, and immune
193 infiltration suggesting DEN-induced carcinogenesis in the mouse liver (**Fig. 1B**).
194 Immunohistochemical analysis showed that positive cells for E-Cadherin were greater in
195 vehicle-treated mice compared to the DEN-treated mice which suggest loss of cellular
196 adhesion and increased proliferation and migration (**Fig. 2A**). The positive area for vimentin
197 were significantly increased in tumor tissue compared with normal tissues (**Figs. 2B and 2C**).
198 These results indicated that the DEN-induced mouse model was successfully constructed
199 with characteristic proliferative features.

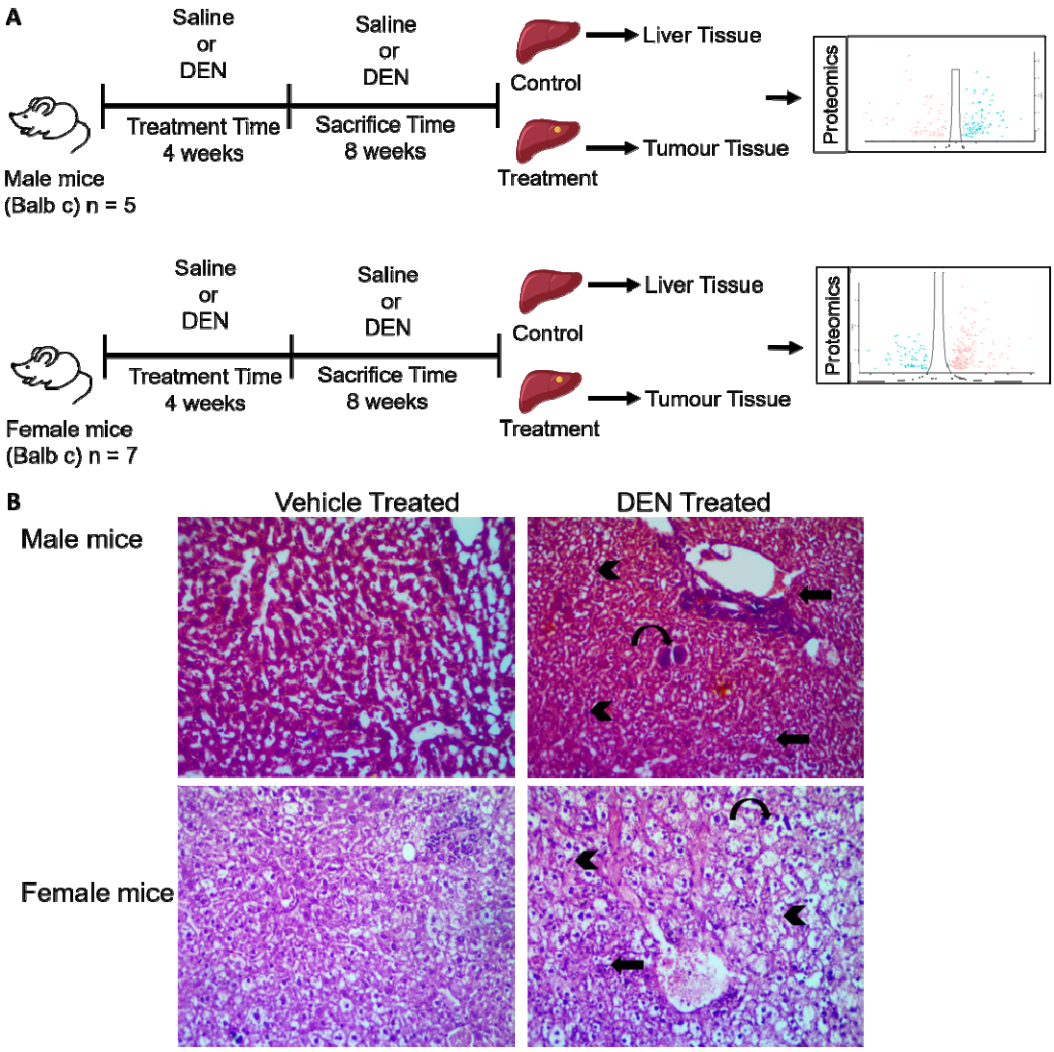

Figure 1. A, Schematic diagram of the development of DEN-induced HCC in Balb/c mice **B,** H&E staining of mouse liver indicating the development of HCC in DEN-treated male and female mice. Half circular arrows indicate enlarged nuclei, arrows indicate immune infiltration and arrow heads show disorganized morphology.

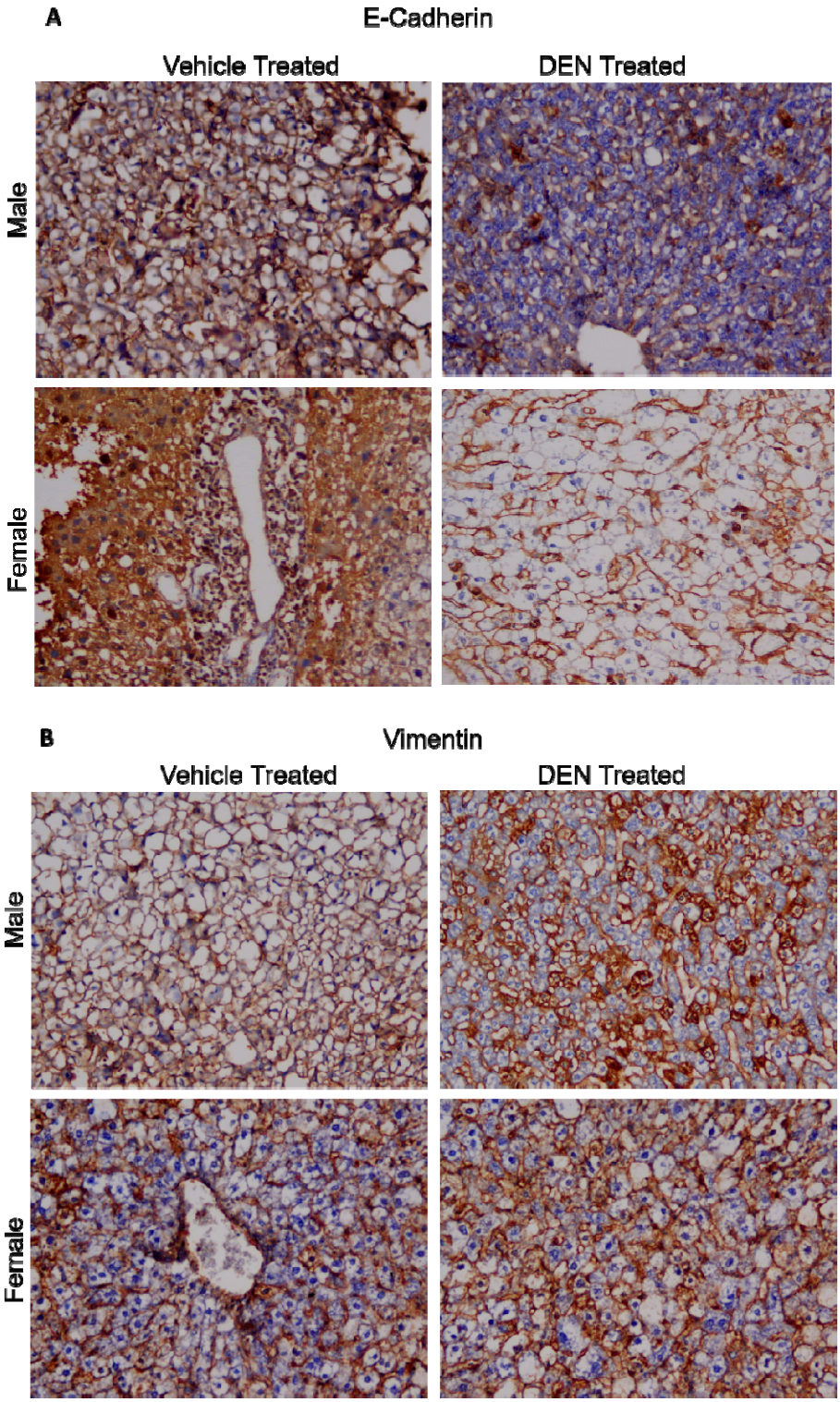

Figure 2. Immunohistochemical (IHC) staining of liver sections from vehicle-treated and DEN-treated mice. **A,** E-Cadherin staining of vehicle-treated, and DEN-treated male/female mice **B,** Vimentin staining of vehicle-treated and DEN-treated male/female mice.

Statistical data analysis

211 In the present study, protein samples isolated from 14 mice were analyzed through
212 label-free LC-MS which led to the identification of total 2897 proteins (Supplementary Table
213 1). After the filtration of potential contaminants, only identified by site and reverse database
214 hits 2803 proteins were selected and divided into four groups (Treated Male Mice, Treated
215 Female Mice, Control Male Mice, and Control Female Mice). From this point onwards, data
216 was segregated gender wise followed by separate Log2 transformation of both male and
217 female LFQ intensities of proteins. Both groups were separately subjected to filtration based
218 on 70% values in each group, reducing the total number of proteins to 1419 and 1049 in
219 males and females respectively. After filtration post hoc Tukey's HSD test for one-way
220 ANOVA was used to test the significance of the expressed protein based on the difference
221 between the LFQ intensities of treatment and control groups. In female mice, 857 proteins
222 were found to be common between treatment and control groups whereas 192 proteins
223 were significantly differentially expressed among which 54 proteins were downregulated
224 (Supplementary Table 2) and 138 proteins were upregulated (Supplementary Table 3). In
225 male mice, 1273 proteins were found to be common between treatment and control groups
226 whereas 146 proteins were found to be significantly differentially expressed among which 61
227 proteins were upregulated (Supplementary Table 4) whereas 85 proteins were
228 downregulated (Supplementary Table 4). Supplementary Tables 2,3,4 and 5 display the
229 protein IDs, gene names, and unique peptides of the altered proteins in the treatment
230 groups of male and female mice.

231 Venn diagrams of gender-wise comparisons indicated that among the upregulated
232 proteins 8 proteins were common between both male and female mice whereas 53 and 130
233 were differentially expressed between male and female mice respectively. Among the
234 downregulated proteins, 2 proteins were common between the male and female mice
235 whereas 83 and 52 proteins were differentially expressed between male and female mice
236 respectively (**Fig. 3 A-C**).

237

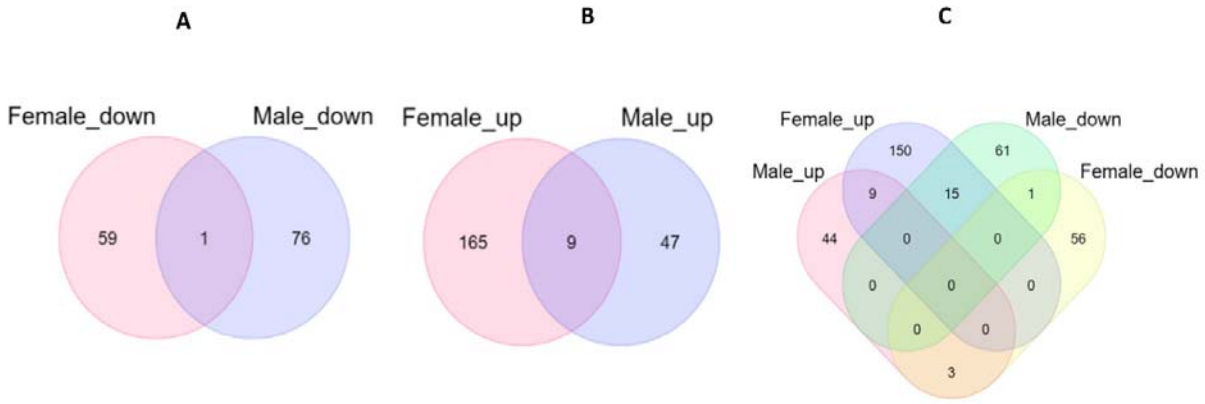

238

239 **Figure 3. A,** Among the significantly downregulated proteins only 1 protein (Indolethylamine
240 N-methyltransferase) was common in both male and female mice. **B,** Among the significantly

upregulated proteins 9 proteins, (Tropomyosin 3, related sequence 7, Nucleolin, Histone H1.2, Tropomyosin alpha-3 chain, Lamina-associated polypeptide 2, Heterogeneous nuclear ribonucleoprotein U, Heterogeneous nuclear ribonucleoprotein M, ES1 protein homolog, mitochondrial were common in both male and Female mice. **C,** Combined representation of common and differentially expressed proteins in treated male and female mice.

Heat maps represent hierarchical clustering and comparison between different samples in both male and female sets (**Fig. 4 A, B**). Principal component analysis (PCA) was carried out to obtain the major features of the data. Control and treated groups were clearly separated on the PCA plot for female mice with 55.3% contribution from component 1 and 15.3% contribution from component 2 (**Fig. 5A**). For the male mice the separation was wider with the control group aligned on the right and treated group aligned on the left vertically, component 1 making 96.9 % contribution while component 2 made 2.3 % contribution (**Fig. 5B**). Volcano plots for male and female sets represent the relationship between FDR and fold change (p-value ≤ 0.05, $|\log2FC| \geq 0.5$) (**Fig. 5 C, D**).

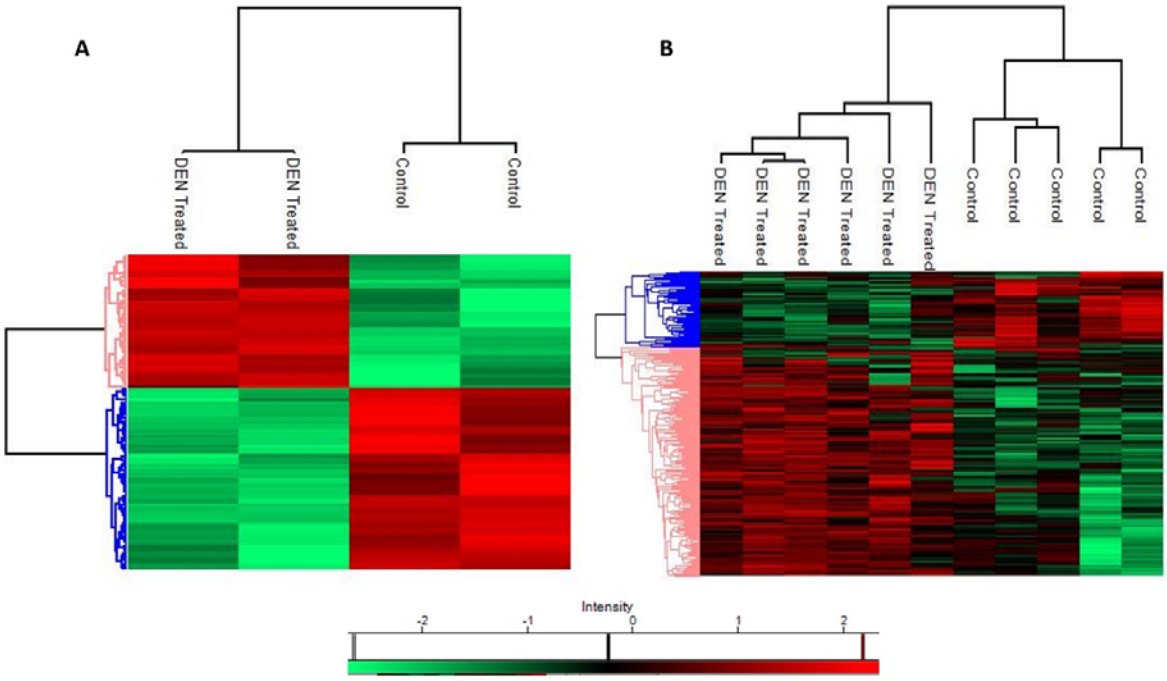

Figure 4. Heatmap of DEPs expression in non-tumor and tumor tissues of **A,** male and **B,** female groups. Perseus software (version 2.0.11.01`1) was used to create a heat map.

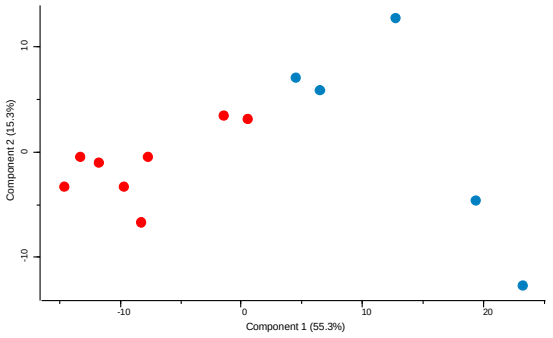
Component 2 (15.3%)
Component 1 (55.3%)

A

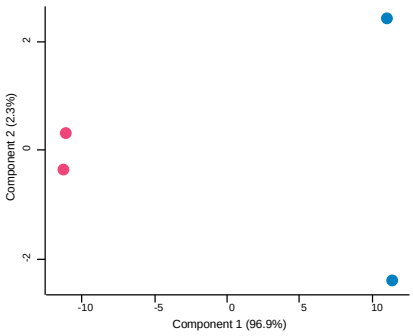
Component 2 (2.3%)
Component 1 (96.9%)

B

C

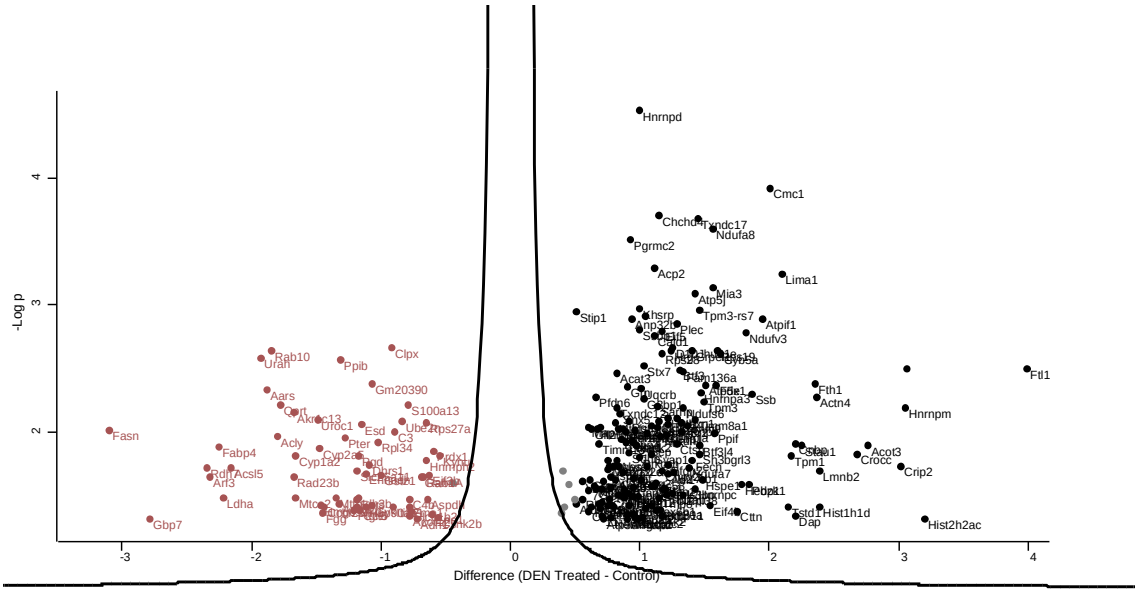
-Log p
Difference (DEN Treated - Control)
Hnrnpd
Cmc1
Pgrmc2
Acp2
Lima1
Stip1
Atpif1
Ndufv3
Ftl1
Fth1
Actn4
Hnrnpm
Acot3
Crocc
Crip2
Lmnb2
Hist2h2ac
Fasn
Gbp7
Ldha
Rab10
Urah
Ppib
Clpx
Gm20390
Aars
S100a13
Fabp4
Acly
Cyp1a2
Rad23b
Arf3
Rdh1
Acsl5
Esd
Pter
Rpl34
Ppif
Tpm1
Ssb
Dap
Cttn
Eif4
Hist1h1d

D

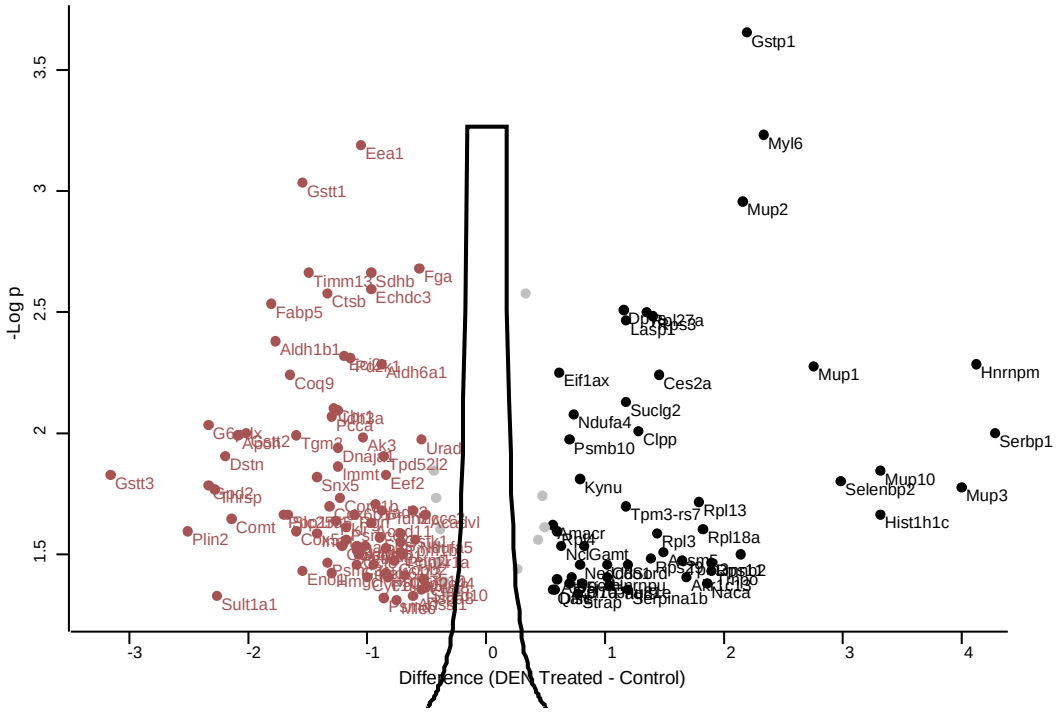

Figure 5. PCA Plots represent the separation between the two components in female **A,** male **B,** groups. The blue color indicates the control group whereas the red color indicates the treatment group. Volcano plot of differentially expressed proteins in female **C,** and male **D,** sets. Brown dots represent down-regulated proteins, black dots represent up-regulated proteins and grey dots represent proteins with insignificant differences.

Enrichment of cytoskeletal, mitochondrial, metabolic and Oxidoreductase Clusters in Females

Functional enrichment analysis (Gene Ontology (GO)), Reactome Analysis, and KEGG pathway analysis) of DEPs was performed to study the biological relevance of significantly altered proteins. First, GO analysis was performed in terms of biological processes (BP), cellular composition (CC), and molecular function (MF) (**Fig. 6 A, B**). The up-regulated proteins in treated female mice were mainly involved in structural constituent of cytoskeleton, protein folding, purine nucleoside triphosphate metabolic process and structural and functional constituents of mitochondria whereas, the downregulated proteins were largely concerned various metabolic and catabolic processes and oxidoreductase activity (**Fig. 6A**).Reactome pathway overrepresentation analysis further revealed that proteins involved in the metabolism of (RNA and protein), caspase-mediated cleavage of cytoskeletal proteins were upregulated in female mice (**Fig. 6C**). Finally, KEGG pathway analysis showed that proteins involved in chemical carcinogenesis and formation of reactive

283 oxygen species, oxidative phosphorylation, nonalcoholic fatty liver disease was upregulated
284 in treated female mice and downregulated in treated male mice whereas proteins involved
285 in Tryptophan metabolism were downregulated in treated female mice and upregulated in
286 treated male mice. Proteins involved in chemical carcinogenesis-DNA adduct, and
287 glutathione metabolism were downregulated in treated male mice whereas genes related to
288 ribosomes, Taurine, hypotaurine metabolism, Pantothenate, and CoA biosynthesis were
289 upregulated in treated male mice. In treated female mice proteins involved in Retinol
290 metabolism, Pyruvate metabolism, Fatty acid degradation, Cysteine and methionine
291 metabolism, Fatty acid metabolism and biosynthesis, Glycolysis / Gluconeogenesis Drug
292 metabolism, cytochrome P450, Alcoholic liver disease were downregulated whereas
293 proteins involved in PARP signaling pathway, cytoskeleton in muscle cells were upregulated.
294 Only one pathway of carbon metabolism was downregulated in both treated male and
295 female mice (**Fig. 6D**).

296 **Enrichment of translational, Ribosomal and Mitochondrial Clusters in Male Mice**

297 The upregulated proteins in treated male mice were related to translation, ribosomal
298 structural and binding subunits and mRNA binding, whereas the downregulated proteins
299 were predominantly related to generation of precursor metabolites, metabolic processes,
300 catabolic processes, glutathione transferase activity, oxidoreductase activity and
301 mitochondrial activity (**Fig. 6B**). Reactome pathway overrepresentation analysis further
302 revealed that in male mice proteins associated with ribosomal processing, translation
303 initiation, dependent and independent nonsense mediated decay, apoptosis and apoptosis
304 induced DNA fragmentation were upregulated whereas proteins involved in fatty acid
305 metabolism, respiratory electron transport chain, cellular response to chemical stress,
306 metabolism of amino acid and derivatives, TP53 regulated metabolic genes, degradation of
307 beta catenin by the destruction complex, apoptotic execution phase, signaling by Rho
308 GTPase, ribosomal scanning and start codon recognition, citric acid cycle, and respiratory
309 electron transport chain were downregulated in treated male mice.

GO Terms Overrepresentation Analysis (Female)
GO Term
protein folding
oxidative phosphorylation
cellular respiration
aerobic respiration
energy derivation by oxidation of organic compounds
proton motive force−driven mitochondrial ATP synthesis
generation of precursor metabolites and energy
proton motive force−driven ATP synthesis
purine nucleoside triphosphate biosynthetic process
purine nucleoside triphosphate metabolic process
inner mitochondrial membrane protein complex
mitochondrial protein−containing complex
mitochondrial intermembrane space
cell cortex
organelle envelope lumen
respiratory chain complex
respirasome
mitochondrial matrix
cortical cytoskeleton
mitochondrial respirasome
actin binding
actin filament binding
mRNA binding
unfolded protein binding
protein−folding chaperone binding
structural constituent of cytoskeleton
protein folding chaperone
isomerase activity
protein−disulfide reductase activity
proton−transporting ATP synthase activity, rotational mechanism
small molecule catabolic process
fatty acid metabolic process
sulfur compound metabolic process
acyl−CoA metabolic process
thioester metabolic process
purine ribonucleotide metabolic process
organic acid catabolic process
carboxylic acid catabolic process
ribonucleotide metabolic process
NAD metabolic process
myelin sheath
peroxisome
microbody
brush border membrane
microvillus membrane
oxidoreductase activity, acting on the CH−OH group of donors, NAD or NADP as acceptor
oxidoreductase activity, acting on CH−OH group of donors
hydro−lyase activity
carbon−oxygen lyase activity
lyase activity
ATP−dependent protein folding chaperone
carboxylic acid binding
thiolester hydrolase activity
NADP binding
organic acid binding
−10
−5
0
5
10
−log10(FDR)
Category
BP
CC
MF

310 **A**

GO Terms Overrepresentation Analysis (Male)
GO Term
cytoplasmic translation
translation at presynapse
translation at synapse
translation at postsynapse
sulfur compound metabolic process
amino acid metabolic process
organic acid biosynthetic process
heterochromatin formation
cellular respiration
cytosolic ribosome
ribosomal subunit
ribosome
cytosolic large ribosomal subunit
large ribosomal subunit
cytosolic small ribosomal subunit
nuclear periphery
nuclear lamina
small ribosomal subunit
tricarboxylic acid cycle enzyme complex
structural constituent of ribosome
rRNA binding
mRNA binding
structural constituent of chromatin
oxidoreductase activity, acting on the aldehyde or oxo group of donors
ligase activity
5S rRNA binding
ribonucleoprotein complex binding
acid−thiol ligase activity
generation of precursor metabolites and energy
energy derivation by oxidation of organic compounds
small molecule catabolic process
aerobic respiration
branched−chain amino acid metabolic process
respiratory electron transport chain
organic acid catabolic process
carboxylic acid catabolic process
glutathione metabolic process
aerobic electron transport chain
mitochondrial protein−containing complex
inner mitochondrial membrane protein complex
mitochondrial respirasome
respiratory chain complex
respirasome
cytochrome complex
peroxisome
microbody
mitochondrial matrix
oxidoreductase complex
fatty acid derivative binding
glutathione transferase activity
oxidoreductase activity, acting on the CH−OH group of donors, NAD or NADP as acceptor
unfolded protein binding
oxidoreductase activity, acting on CH−OH group of donors
lyase activity
magnesium ion binding
transferase activity, transferring alkyl or aryl (other than methyl) groups
fatty−acyl−CoA binding
acyl−CoA binding
−10
−5
0
5
10
−log10(FDR)
Category
BP
CC
MF

311 **B**

C

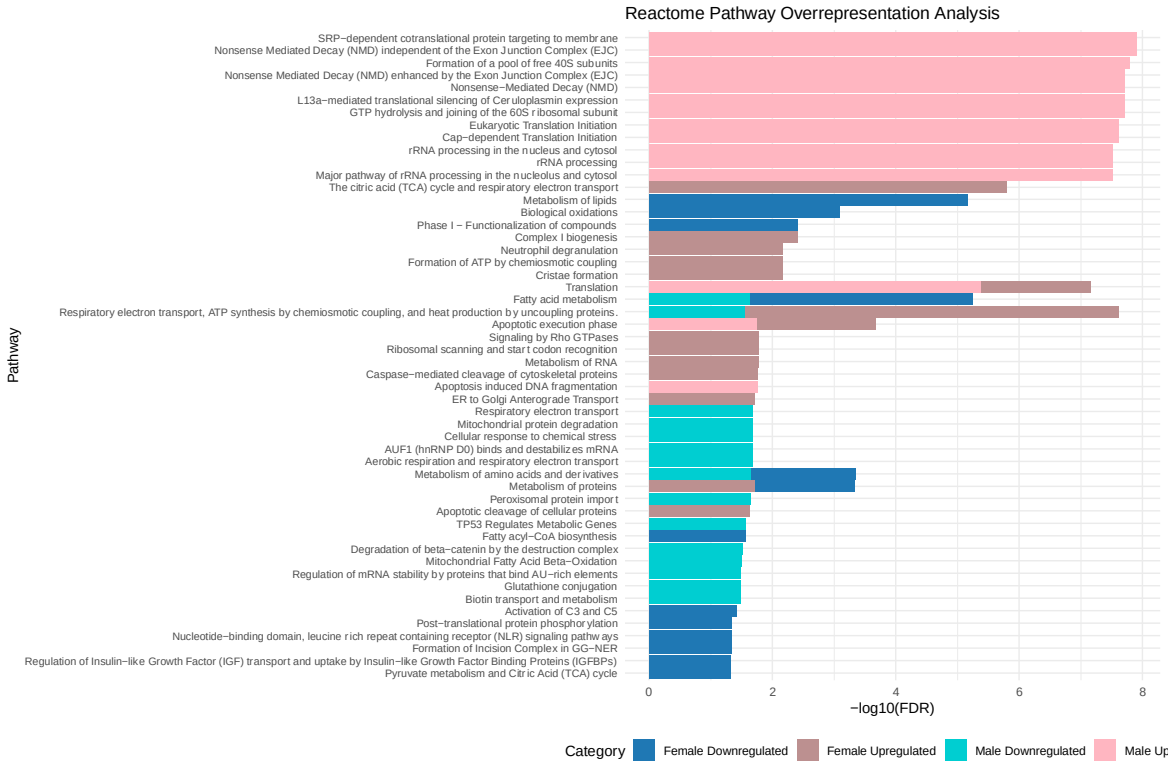

D

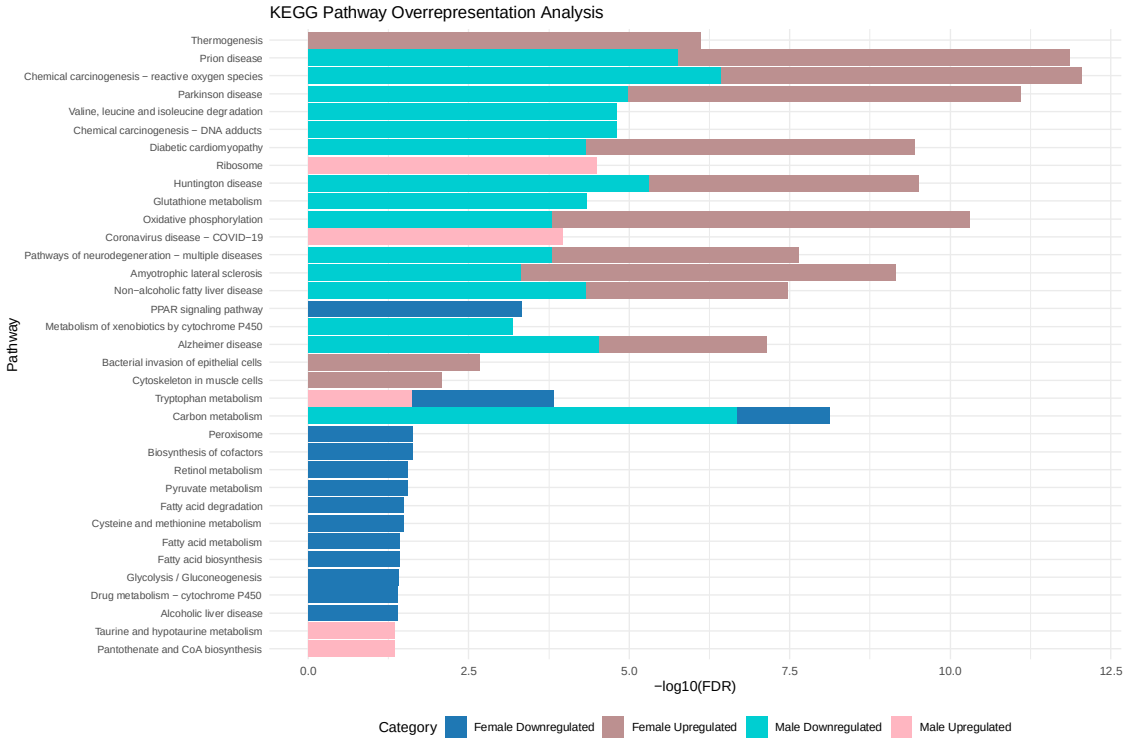

Figure 6. Overrepresentation Analysis **A,** GO term Analysis of female mice **B,** GO term analysis of male mice **C,** Reactome Analysis of DEN-treated male and female mice **D,** KEG pathway Analysis of DEN-treated male and female mice.

319 **PPI networks in Male and Female mice**

320 For DEPs in male and female mice, the PPI network was constructed using the
321 STRING database and Cytoscape. The male PPI network consisted of 108 nodes with 922
322 edges while the female PPI network contained 217 nodes with 2042 edges (**Fig. 7 A, B**). The
323 significant module for each network was obtained by MCODE using default parameters.
324 MCODE score of the top modules was 13.538 (male) and 14.571 (female) (**Fig. 8 A, B**).
325 Moreover, the MCC method was used to select hub genes from the PPI network using the
326 CytoHubba plugin of Cytoscape. In the male cluster top ten genes ranked by highest maximal
327 clique centrality (MCC) were Rpl13, Rpl4, Eef2, Rps11, Rpl18a, Serbp1, Rpl27a, Rpl3, Rpl7a
328 and Rps3. These were identified as hub genes for the male network (**Fig. 9A**). For the female
329 cluster Hub genes were identified to be Uqcrb, Cox6b1, Ndufc2, Ndufa8, Sdhb, Atp5d,
330 Ndufa7, Ndufa2 and Ndufs6 (**Fig. 9B**). Over representation analysis of hub genes is indicated
331 in **Figure 9C.**

332

333

334

A

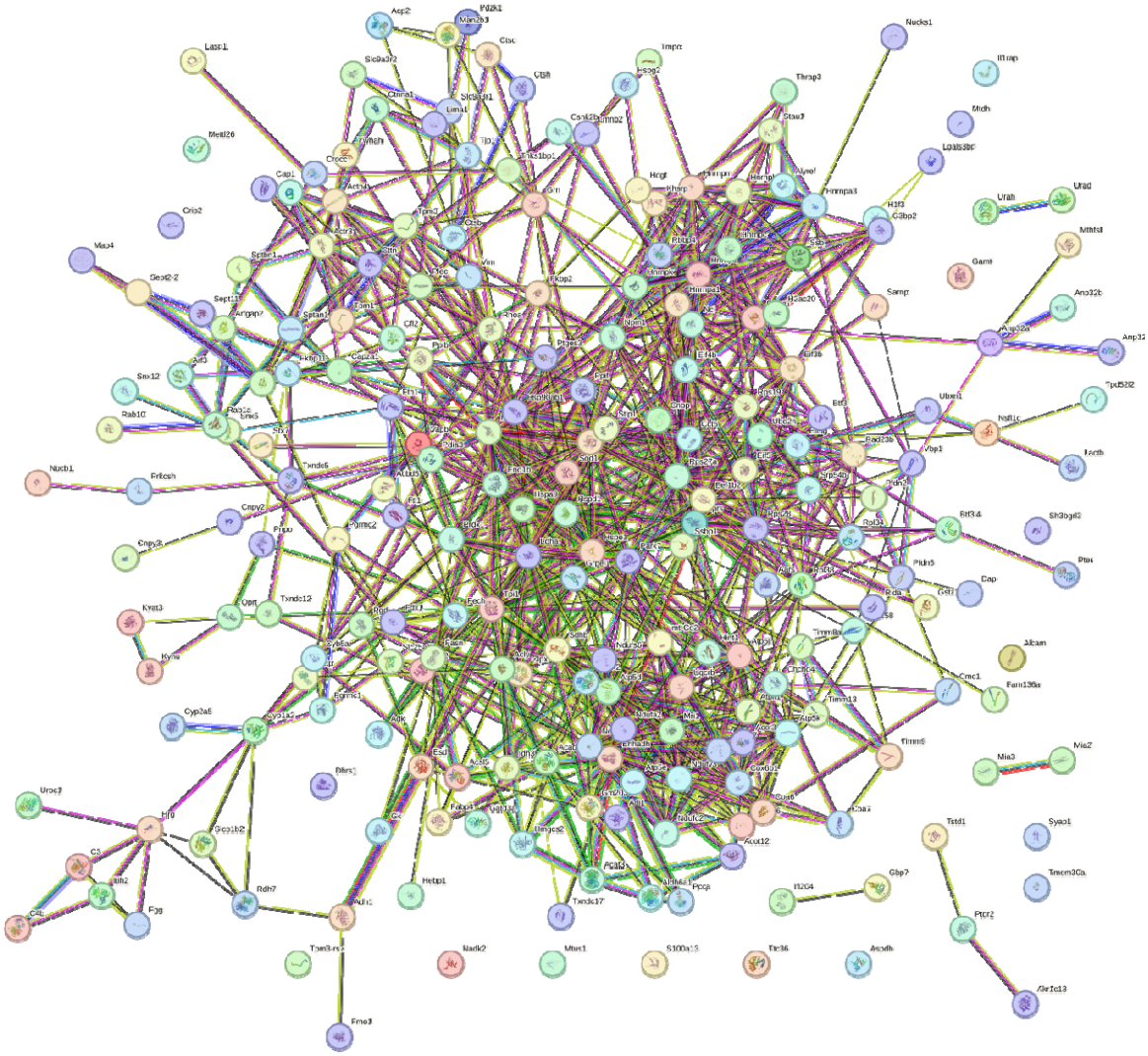
Pdzk1
Nucks1
Lase1
Mettl26
Cric2
Mat4
Nucb1
Cyp2a5
Urod
Tsfd1
Syap1
Tmem30a
Ptcr2
Zfp704
Gbp7
Mia3
Mia2
Ccdc13
Fmo3
Mark2
Mtor1
S100a13
Tlr36
Ascdh
Hetpl
Rdh7
Fgg
Cd4
Cp
Kynu
Kyat3
Cmpx2
Cmpx3
Frkcsh
Rab10
Snx12
Sept11
Sesn2-2
Argap7
Cap1
Crocc
Lim1
Slc9a3r2
Aep2
Cisc
Cfdh
Impc
Thrap3
Stau1
Mtdh
Loaiss8c
Urah
Mmrsl
Gamt
Amp32b
Amp32
Tpd52l2
Ubxn1
Nsfl1c
Ikzdh
Vbp1
Rtf3d
Sh3bgd2
Ptx
Cap
Ldcam
Fam136a
Cmc1
Tmem8
Tmem13
Tmem8a
Cyp51a1
Cyp51a2
Esd
Acot12
Pcaf
Ppcp
Tmem2
Tmem4
Tmem5
Tmem6
Tmem7
Tmem9
Tmem10
Tmem11
Tmem12
Tmem14
Tmem15
Tmem16
Tmem17
Tmem18
Tmem19
Tmem20
Tmem21
Tmem22
Tmem23
Tmem24
Tmem25
Tmem26
Tmem27
Tmem28
Tmem29
Tmem30
Tmem31
Tmem32
Tmem33
Tmem34
Tmem35
Tmem36
Tmem37
Tmem38
Tmem39
Tmem40
Tmem41
Tmem42
Tmem43
Tmem44
Tmem45
Tmem46
Tmem47
Tmem48
Tmem49
Tmem50
Tmem51
Tmem52
Tmem53
Tmem54
Tmem55
Tmem56
Tmem57
Tmem58
Tmem59
Tmem60
Tmem61
Tmem62
Tmem63
Tmem64
Tmem65
Tmem66
Tmem67
Tmem68
Tmem69
Tmem70
Tmem71
Tmem72
Tmem73
Tmem74
Tmem75
Tmem76
Tmem77
Tmem78
Tmem79
Tmem80
Tmem81
Tmem82
Tmem83
Tmem84
Tmem85
Tmem86
Tmem87
Tmem88
Tmem89
Tmem90
Tmem91
Tmem92
Tmem93
Tmem94
Tmem95
Tmem96
Tmem97
Tmem98
Tmem99
Tmem100
Tmem101
Tmem102
Tmem103
Tmem104
Tmem105
Tmem106
Tmem107
Tmem108
Tmem109
Tmem110
Tmem111
Tmem112
Tmem113
Tmem114
Tmem115
Tmem116
Tmem117
Tmem118
Tmem119
Tmem120
Tmem121
Tmem122
Tmem123
Tmem124
Tmem125
Tmem126
Tmem127
Tmem128
Tmem129
Tmem130
Tmem131
Tmem132
Tmem133
Tmem134
Tmem135
Tmem136
Tmem137
Tmem138
Tmem139
Tmem140
Tmem141
Tmem142
Tmem143
Tmem144
Tmem145
Tmem146
Tmem147
Tmem148
Tmem149
Tmem150
Tmem151
Tmem152
Tmem153
Tmem154
Tmem155
Tmem156
Tmem157
Tmem158
Tmem159
Tmem160
Tmem161
Tmem162
Tmem163
Tmem164
Tmem165
Tmem166
Tmem167
Tmem168
Tmem169
Tmem170
Tmem171
Tmem172
Tmem173
Tmem174
Tmem175
Tmem176
Tmem177
Tmem178
Tmem179
Tmem180
Tmem181
Tmem182
Tmem183
Tmem184
Tmem185
Tmem186
Tmem187
Tmem188
Tmem189
Tmem190
Tmem191
Tmem192
Tmem193
Tmem194
Tmem195
Tmem196
Tmem197
Tmem198
Tmem199
Tmem200
Tmem201
Tmem202
Tmem203
Tmem204
Tmem205
Tmem206
Tmem207
Tmem208
Tmem209
Tmem210
Tmem211
Tmem212
Tmem213
Tmem214
Tmem215
Tmem216
Tmem217
Tmem218
Tmem219
Tmem220
Tmem221
Tmem222
Tmem223
Tmem224
Tmem225
Tmem226
Tmem227
Tmem228
Tmem229
Tmem230
Tmem231
Tmem232
Tmem233
Tmem234
Tmem235
Tmem236
Tmem237
Tmem238
Tmem239
Tmem240
Tmem241
Tmem242
Tmem243
Tmem244
Tmem245
Tmem246
Tmem247
Tmem248
Tmem249
Tmem250
Tmem251
Tmem252
Tmem253
Tmem254
Tmem255
Tmem256
Tmem257
Tmem258
Tmem259
Tmem260
Tmem261
Tmem262
Tmem263
Tmem264
Tmem265
Tmem266
Tmem267
Tmem268
Tmem269
Tmem270
Tmem271
Tmem272
Tmem273
Tmem274
Tmem275
Tmem276
Tmem277
Tmem278
Tmem279
Tmem280
Tmem281
Tmem282
Tmem283
Tmem284
Tmem285
Tmem286
Tmem287
Tmem288
Tmem289
Tmem290
Tmem291
Tmem292
Tmem293
Tmem294
Tmem295
Tmem296
Tmem297
Tmem298
Tmem299
Tmem300
Tmem301
Tmem302
Tmem303
Tmem304
Tmem305
Tmem306
Tmem307
Tmem308
Tmem309
Tmem310
Tmem311
Tmem312
Tmem313
Tmem314
Tmem315
Tmem316
Tmem317
Tmem318
Tmem319
Tmem320
Tmem321
Tmem322
Tmem323
Tmem324
Tmem325
Tmem326
Tmem327
Tmem328
Tmem329
Tmem330
Tmem331
Tmem332
Tmem333
Tmem334
Tmem335
Tmem336
Tmem337
Tmem338
Tmem339
Tmem340
Tmem341
Tmem342
Tmem343
Tmem344
Tmem345
Tmem346
Tmem347
Tmem348
Tmem349
Tmem350
Tmem351
Tmem352
Tmem353
Tmem354
Tmem355
Tmem356
Tmem357
Tmem358
Tmem359
Tmem360
Tmem361
Tmem362
Tmem363
Tmem364
Tmem365
Tmem366
Tmem367
Tmem368
Tmem369
Tmem370
Tmem371
Tmem372
Tmem373
Tmem374
Tmem375
Tmem376
Tmem377
Tmem378
Tmem379
Tmem380
Tmem381
Tmem382
Tmem383
Tmem384
Tmem385
Tmem386
Tmem387
Tmem388
Tmem389
Tmem390
Tmem391
Tmem392
Tmem393
Tmem394
Tmem395
Tmem396
Tmem397
Tmem398
Tmem399
Tmem400
Tmem401
Tmem402
Tmem403
Tmem404
Tmem405
Tmem406
Tmem407
Tmem408
Tmem409
Tmem410
Tmem411
Tmem412
Tmem413
Tmem414
Tmem415
Tmem416
Tmem417
Tmem418
Tmem419
Tmem420
Tmem421
Tmem422
Tmem423
Tmem424
Tmem425
Tmem426
Tmem427
Tmem428
Tmem429
Tmem430
Tmem431
Tmem432
Tmem433
Tmem434
Tmem435
Tmem436
Tmem437
Tmem438
Tmem439
Tmem440
Tmem441
Tmem442
Tmem443
Tmem444
Tmem445
Tmem446
Tmem447
Tmem448
Tmem449
Tmem450
Tmem451
Tmem452
Tmem453
Tmem454
Tmem455
Tmem456
Tmem457
Tmem458
Tmem459
Tmem460
Tmem461
Tmem462
Tmem463
Tmem464
Tmem465
Tmem466
Tmem467
Tmem468
Tmem469
Tmem470
Tmem471
Tmem472
Tmem473
Tmem474
Tmem475
Tmem476
Tmem477
Tmem478
Tmem479
Tmem480
Tmem481
Tmem482
Tmem483
Tmem484
Tmem485
Tmem486
Tmem487
Tmem488
Tmem489
Tmem490
Tmem491
Tmem492
Tmem493
Tmem494
Tmem495
Tmem496
Tmem497
Tmem498
Tmem499
Tmem500
Tmem501
Tmem502
Tmem503
Tmem504
Tmem505
Tmem506
Tmem507
Tmem508
Tmem509
Tmem510
Tmem511
Tmem512
Tmem513
Tmem514
Tmem515
Tmem516
Tmem517
Tmem518
Tmem519
Tmem520
Tmem521
Tmem522
Tmem523
Tmem524
Tmem525
Tmem526
Tmem527
Tmem528
Tmem529
Tmem530
Tmem531
Tmem532
Tmem533
Tmem534
Tmem535
Tmem536
Tmem537
Tmem538
Tmem539
Tmem540
Tmem541
Tmem542
Tmem543
Tmem544
Tmem545
Tmem546
Tmem547
Tmem548
Tmem549
Tmem550
Tmem551
Tmem552
Tmem553
Tmem554
Tmem555
Tmem556
Tmem557
Tmem558
Tmem559
Tmem560
Tmem561
Tmem562
Tmem563
Tmem564
Tmem565
Tmem566
Tmem567
Tmem568
Tmem569
Tmem570
Tmem571
Tmem572
Tmem573
Tmem574
Tmem575
Tmem576
Tmem577
Tmem578
Tmem579
Tmem580
Tmem581
Tmem582
Tmem583
Tmem584
Tmem585
Tmem586
Tmem587
Tmem588
Tmem589
Tmem590
Tmem591
Tmem592
Tmem593
Tmem594
Tmem595
Tmem596
Tmem597
Tmem598
Tmem599
Tmem600
Tmem601
Tmem602
Tmem603
Tmem604
Tmem605
Tmem606
Tmem607
Tmem608
Tmem609
Tmem610
Tmem611
Tmem612
Tmem613
Tmem614
Tmem615
Tmem616
Tmem617
Tmem618
Tmem619
Tmem620
Tmem621
Tmem622
Tmem623
Tmem624
Tmem625
Tmem626
Tmem627
Tmem628
Tmem629
Tmem630
Tmem631
Tmem632
Tmem633
Tmem634
Tmem635
Tmem636
Tmem637
Tmem638
Tmem639
Tmem640
Tmem641
Tmem642
Tmem643
Tmem644
Tmem645
Tmem646
Tmem647
Tmem648
Tmem649
Tmem650
Tmem651
Tmem652
Tmem653
Tmem654
Tmem655
Tmem656
Tmem657
Tmem658
Tmem659
Tmem660
Tmem661
Tmem662
Tmem663
Tmem664
Tmem665
Tmem666
Tmem667
Tmem668
Tmem669
Tmem670
Tmem671
Tmem672
Tmem673
Tmem674
Tmem675
Tmem676
Tmem677
Tmem678
Tmem679
Tmem680
Tmem681
Tmem682
Tmem683
Tmem684
Tmem685
Tmem686
Tmem687
Tmem688
Tmem689
Tmem690
Tmem691
Tmem692
Tmem693
Tmem694
Tmem695
Tmem696
Tmem697
Tmem698
Tmem699
Tmem700
Tmem701
Tmem702
Tmem703
Tmem704
Tmem705
Tmem706
Tmem707
Tmem708
Tmem709
Tmem710
Tmem711
Tmem712
Tmem713
Tmem714
Tmem715
Tmem716
Tmem717
Tmem718
Tmem719
Tmem720
Tmem721
Tmem722
Tmem723
Tmem724
Tmem725
Tmem726
Tmem727
Tmem728
Tmem729
Tmem730
Tmem731
Tmem732
Tmem733
Tmem734
Tmem735
Tmem736
Tmem737
Tmem738
Tmem739
Tmem740
Tmem741
Tmem742
Tmem743
Tmem744
Tmem745
Tmem746
Tmem747
Tmem748
Tmem749
Tmem750
Tmem751
Tmem752
Tmem753
Tmem754
Tmem755
Tmem756
Tmem757
Tmem758
Tmem759
Tmem760
Tmem761
Tmem762
Tmem763
Tmem764
Tmem765
Tmem766
Tmem767
Tmem768
Tmem769
Tmem770
Tmem771
Tmem772
Tmem773
Tmem774
Tmem775
Tmem776
Tmem777
Tmem778
Tmem779
Tmem780
Tmem781
Tmem782
Tmem783
Tmem784
Tmem785
Tmem786
Tmem787
Tmem788
Tmem789
Tmem790
Tmem791
Tmem792
Tmem793
Tmem794
Tmem795
Tmem796
Tmem797
Tmem798
Tmem799
Tmem800
Tmem801
Tmem802
Tmem803
Tmem804
Tmem805
Tmem806
Tmem807
Tmem808
Tmem809
Tmem810
Tmem811
Tmem812
Tmem813
Tmem814
Tmem815
Tmem816
Tmem817
Tmem818
Tmem819
Tmem820
Tmem821
Tmem822
Tmem823
Tmem824
Tmem825
Tmem826
Tmem827
Tmem828
Tmem829
Tmem830
Tmem831
Tmem832
Tmem833
Tmem834
Tmem835
Tmem836
Tmem837
Tmem838
Tmem839
Tmem840
Tmem841
Tmem842
Tmem843
Tmem844
Tmem845
Tmem846
Tmem847
Tmem848
Tmem849
Tmem850
Tmem851
Tmem852
Tmem853
Tmem854
Tmem855
Tmem856
Tmem857
Tmem858
Tmem859
Tmem860
Tmem861
Tmem862
Tmem863
Tmem864
Tmem865
Tmem866
Tmem867
Tmem868
Tmem869
Tmem870
Tmem871
Tmem872
Tmem873
Tmem874
Tmem875
Tmem876
Tmem877
Tmem878
Tmem879
Tmem880
Tmem881
Tmem882
Tmem883
Tmem884
Tmem885
Tmem886
Tmem887
Tmem888
Tmem889
Tmem890
Tmem891
Tmem892
Tmem893
Tmem894
Tmem895
Tmem896
Tmem897
Tmem898
Tmem899
Tmem900
Tmem901
Tmem902
Tmem903
Tmem904
Tmem905
Tmem906
Tmem907
Tmem908
Tmem909
Tmem910
Tmem911
Tmem912
Tmem913
Tmem914
Tmem915
Tmem916
Tmem917
Tmem918
Tmem919
Tmem920
Tmem921
Tmem922
Tmem923
Tmem924
Tmem925
Tmem926
Tmem927
Tmem928
Tmem929
Tmem930
Tmem931
Tmem932
Tmem933
Tmem934
Tmem935
Tmem936
Tmem937
Tmem938
Tmem939
Tmem940
Tmem941
Tmem942
Tmem943
Tmem944
Tmem945
Tmem946
Tmem947
Tmem948
Tmem949
Tmem950
Tmem951
Tmem952
Tmem953
Tmem954
Tmem955
Tmem956
Tmem957
Tmem958
Tmem959
Tmem960
Tmem961
Tmem962
Tmem963
Tmem964
Tmem965
Tmem966
Tmem967
Tmem968
Tmem969
Tmem970
Tmem971
Tmem972
Tmem973
Tmem974
Tmem975
Tmem976
Tmem977
Tmem978
Tmem979
Tmem980
Tmem981
Tmem982
Tmem983
Tmem984
Tmem985
Tmem986
Tmem987
Tmem988
Tmem989
Tmem990
Tmem991
Tmem992
Tmem993
Tmem994
Tmem995
Tmem996
Tmem997
Tmem998
Tmem999
Tmem1000

336

B

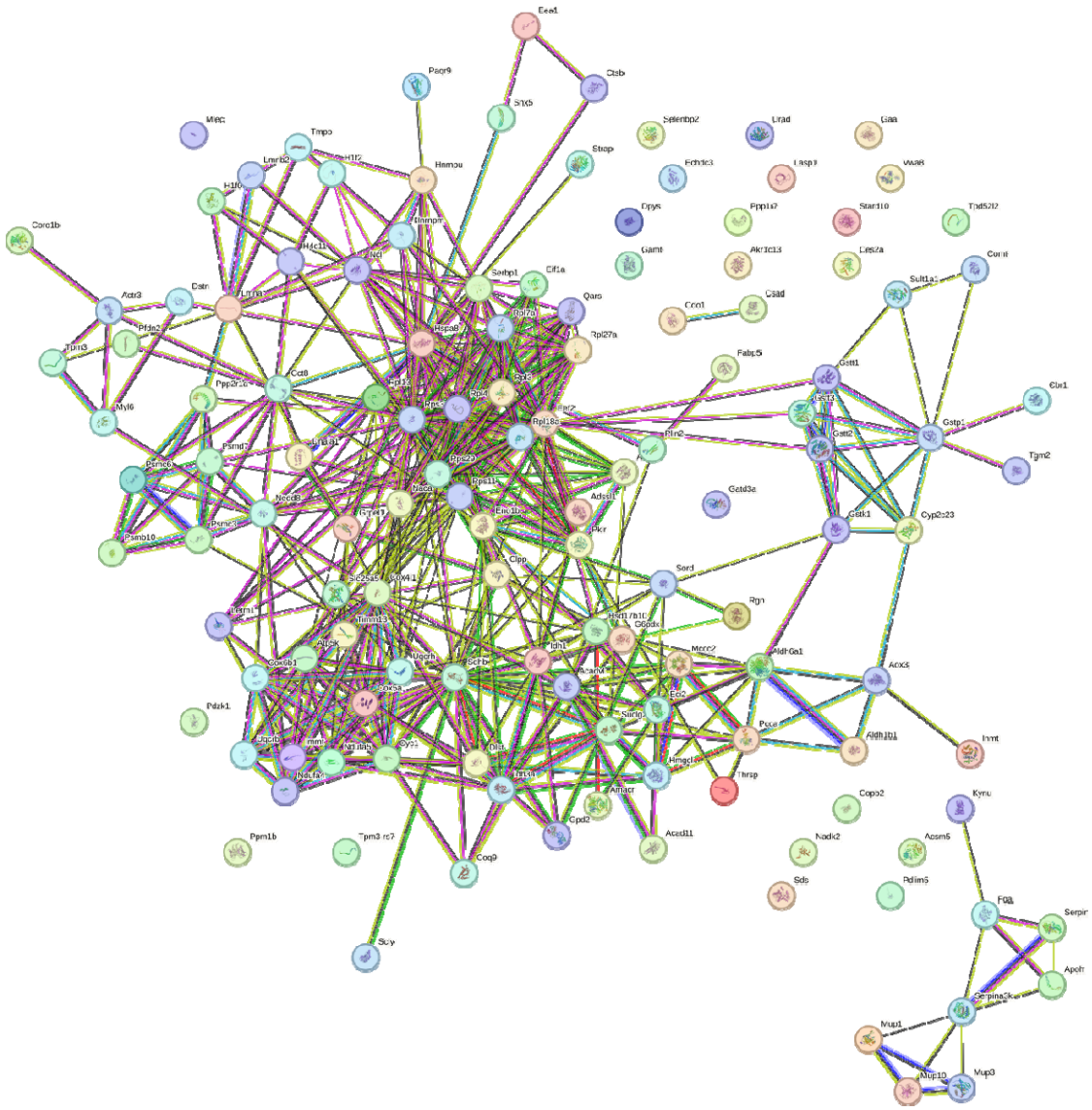
Eea1
Ctsb
Pacr9
Stx5b
Selenbp2
Urad
Gaa
Stoop
Lasp1
Vaa8
Drys
Ppp1r2
Star110
Tnd5f2
Gamt
Akr1c13
Lrs2a
Sult1a1
Gsad
Fabp5
Gstt1
Gstp1
Tgm2
Gstd3a
Gstk1
Cyp2c23
Sord
Rgn
Aldh6a1
Acx3
Aldh1b1
Hmt
Thrsp
Copo2
Kynu
Nadk2
Acsm5
Sds
Pdlim5
Fga
Serpin
Apoh
Serpina3k
Mup1
Mup10
Mup9
Ppm1b
Coq9
Acsd11
Cpd2
Amacr
Hmgcl6
Pcca
Ecs
Mccc2
Idh1
Pdzk1
Myl6
Psmb10
Psmd7
Ccd8
Ppp2r5e
Pdia2
Tpm3
Acta2
Cstr
Lmna
Coro1b
Hmgcr
Hmgcs1
Hmgcs2
Hmgcl
Hmgcs2
Hmgcl
Hmgcl
Hmgcl

A

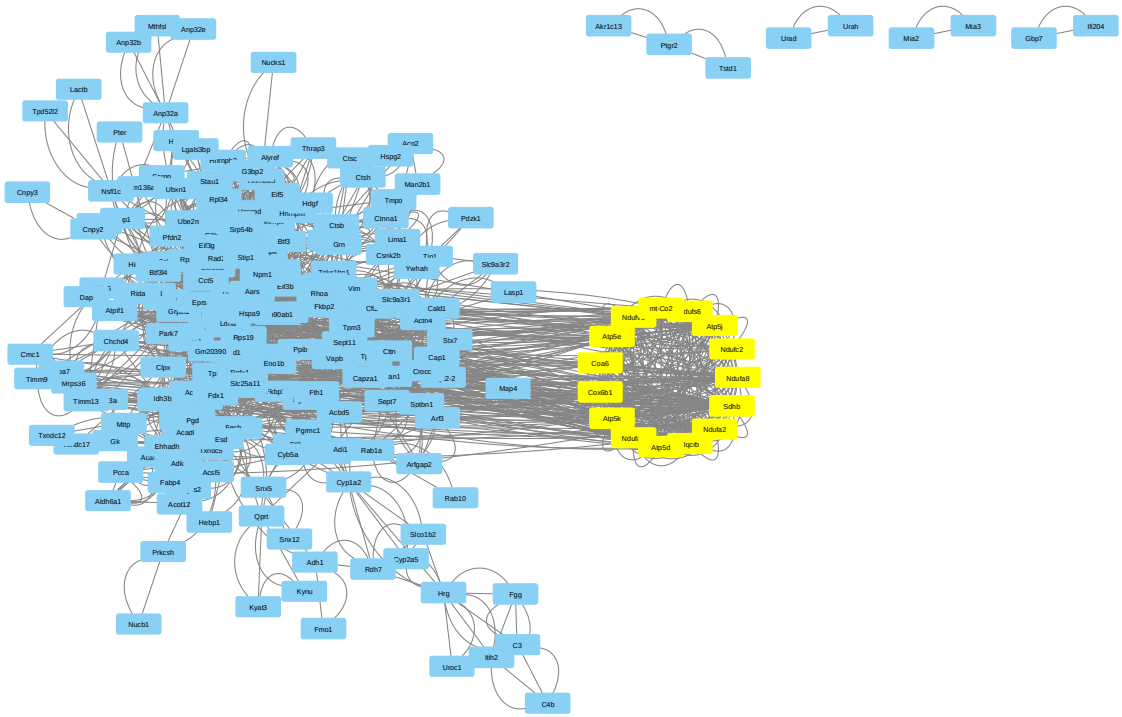
Akr1c13
Ptgr2
Tsid1
Urad
Urah
Mia2
Mia3
Gbp7
Ifit204
Nucks1
Lactb
Tpd52l2
Anp32a
Anp32b
Mthfsl
Anp32e
Pter
Cnpy3
Cnpy2
Pdzk1
Slc9a3r2
Lasp1
Map4
Sdhb
Ndufa8
Ndufc2
Atp5e
Coa6
Coxfdb1
Atp5k
Ndufa5
Atp5d
Igcb
Atp5j
Cmc1
Timm9
Timm13
Txndc12
Pcca
Aldh6a1
Prkcsh
Nucb1
Kyat3
Kynu
Fmo1
Hrg
Fgg
C3
Itih2
Uroc1
C4b
Rab10
Arfgap2
Slco1b2
Cyp2a5
Rdh7
Cyp1a2
Snx5
Qpct
Hebp1
Snx12
Adh1
Rab1a
Adl1
Cyb5a
Pgd
Esd
Ehhadh
Adk
Acsl5
Fabp4
Acot12
Mttp
Gk
Idh3b
Fdx1
Slc25a11
Eno1b
Ppib
Vapb
Sept11
Tpm3
Rps19
Park7
Chchd4
Clpx
Gm20390
Slc9a3r1
Rhoa
Vim
Fkbp2
Cald1
Actn4
Stx7
Cap1
Ciroc
Capza1
Sqstbn1
Sept7
Arf3
Acbd5
Pgrmc1
Fth1
Ctsc
Hspg2
Man2b1
Ctsb
Ctnna1
Lima1
Csnk2b
Ywhah
Grn
Tmpo
Hdgf
Eif5
Rpl34
Ubxn1
Ube2n
Srp54b
Btf3
Slip1
Npm1
Eif3b
Aars
Epsr
Hspa9
Rps19
Ldha
Cct5
Rida
Atpif1
Dap
Bfl34
Eif3g
Pfdn2
Rp
Rad
Ubl4a
Ubl5
Ubl7
Ubl3
Ubl4b
Ubl6
Ubl7
Ubl3
Ubl4b
Ubl6
Ubl7
Ubl3
Ubl4b
Ubl6

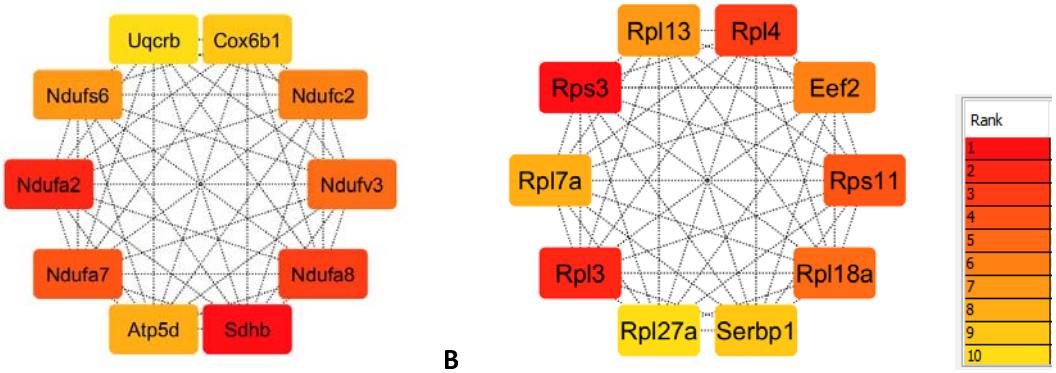

A **B**

C

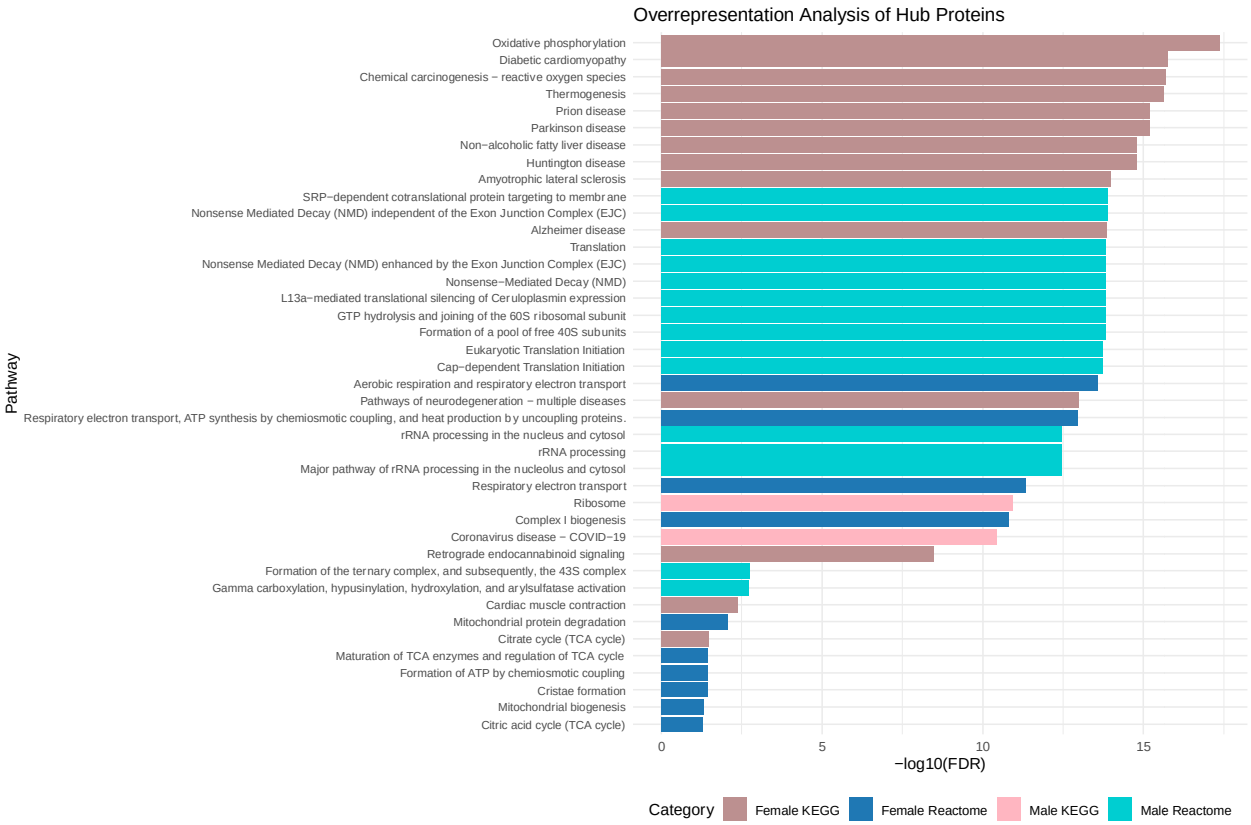

Figure 9. A, Hub gene analysis of DEN-treated female mice, **B,** Hub gene analysis of DEN-treated male mice **C,** ORA of hub genes in both DEN-treated male and female mice.

Prognostic value of RNA Binding and Ribosomal Proteins in Male Mice and mitochondrial Protein NDUFA8 in Female mice

To identify the relationship between expression of Hub protein and overall survival time of patients and to evaluate prognostic value of Hub proteins, survival analysis of human homologs of all Hub genes was carried out using online tool UCLAN. The results indicated

357 that six hub genes were significantly associated with overall poor patient survival. Among
358 the hub genes of DEN-treated female mice only the upregulation of NDUFA8 ($P < 0.017$) was
359 associated with poor patient survival (**Fig. 10A**). In DEN-treated male mice downregulation
360 of EEF2 ($P < 0.022$) and upregulation of RPL7A ($P < 0.0031$), RPL18A ($P < 0.003$), RPL27A ($P <$
361 0.023), RPS3 ($P < 0.016$), RPS 11 ($P < 0.004$) and SERBP1 ($P < 0.0029$) was associated with
362 poor patient survival (**Fig. 10 B-H**).

363

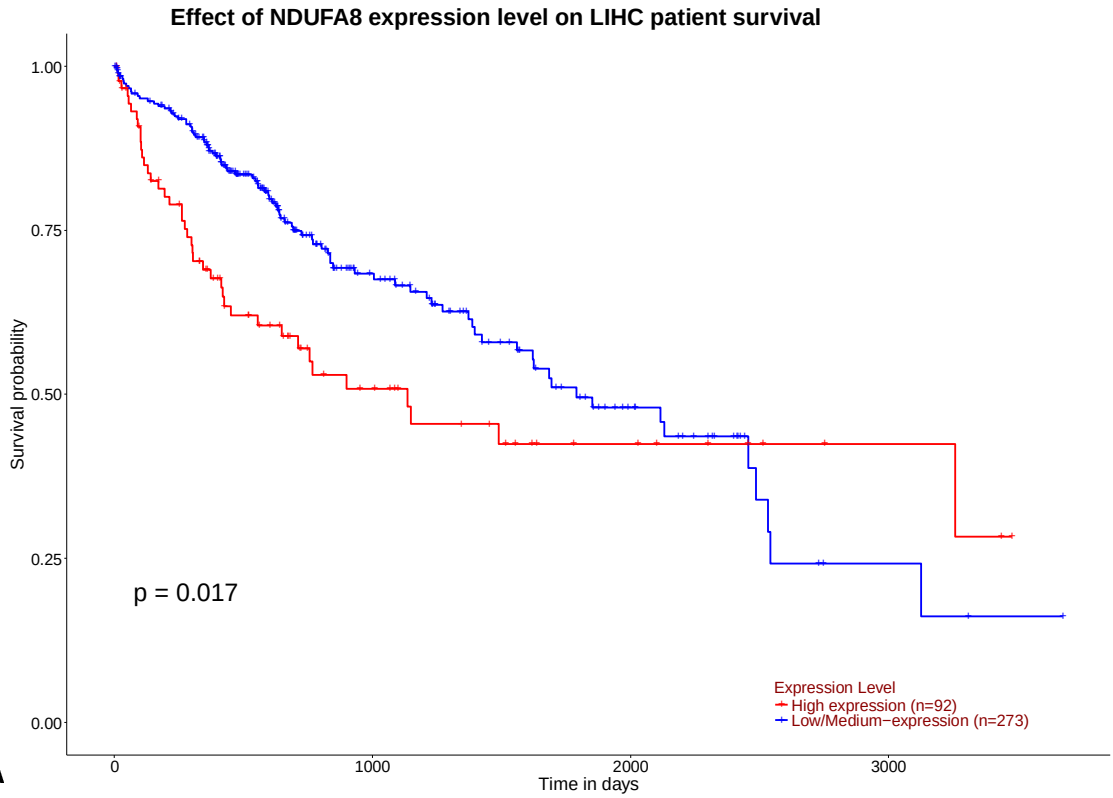
Effect of NDUFA8 expression level on LIHC patient survival
Survival probability
1.00
0.75
0.50
0.25
0.00
p = 0.017
Expression Level
High expression (n=92)
Low/Medium−expression (n=273)
0
1000
2000
3000
Time in days

A

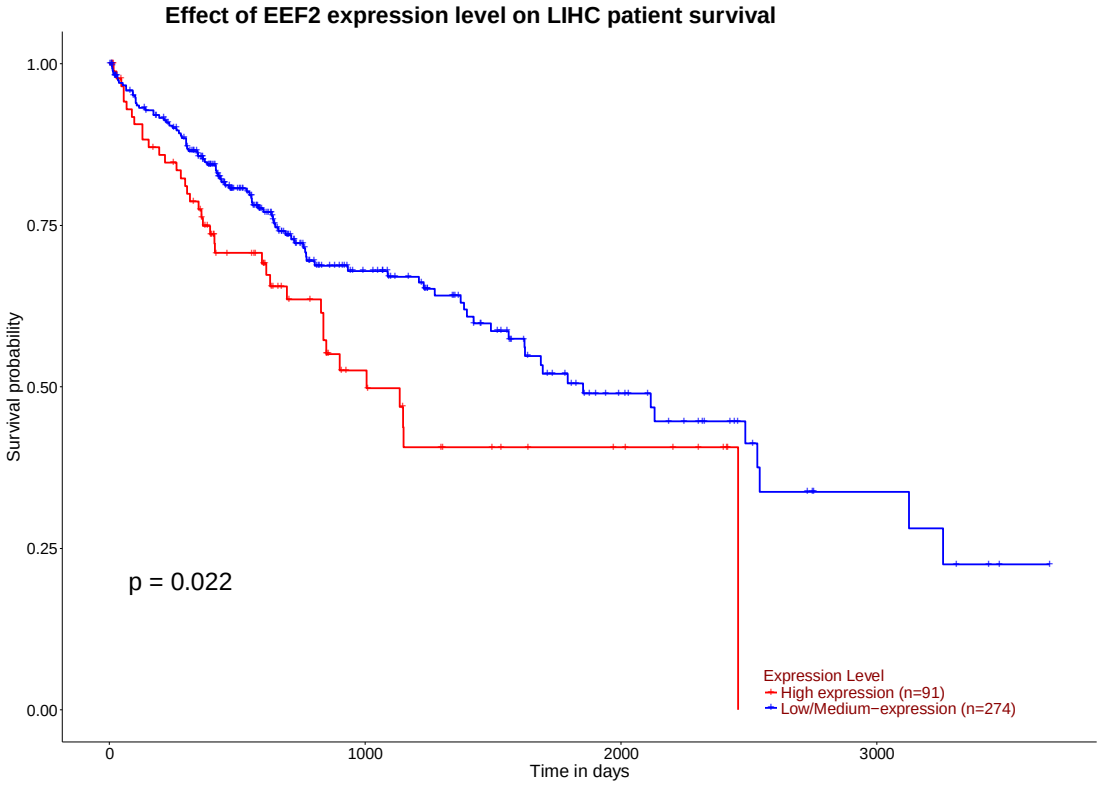
Effect of EEF2 expression level on LIHC patient survival
Survival probability
1.00
0.75
0.50
0.25
0.00
p = 0.022
Expression Level
High expression (n=91)
Low/Medium−expression (n=274)
0
1000
2000
3000
Time in days

B

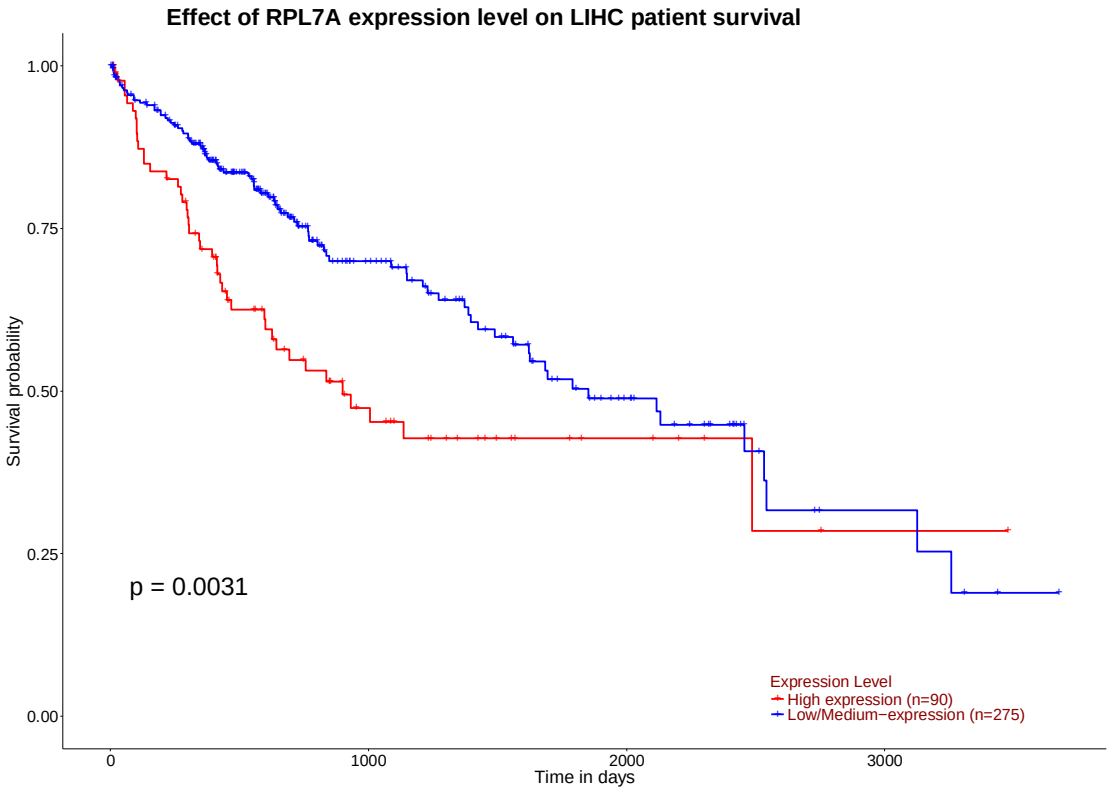
Effect of RPL7A expression level on LIHC patient survival
Survival probability
1.00
0.75
0.50
0.25
0.00
p = 0.0031
Expression Level
High expression (n=90)
Low/Medium−expression (n=275)
0
1000
2000
3000
Time in days

C

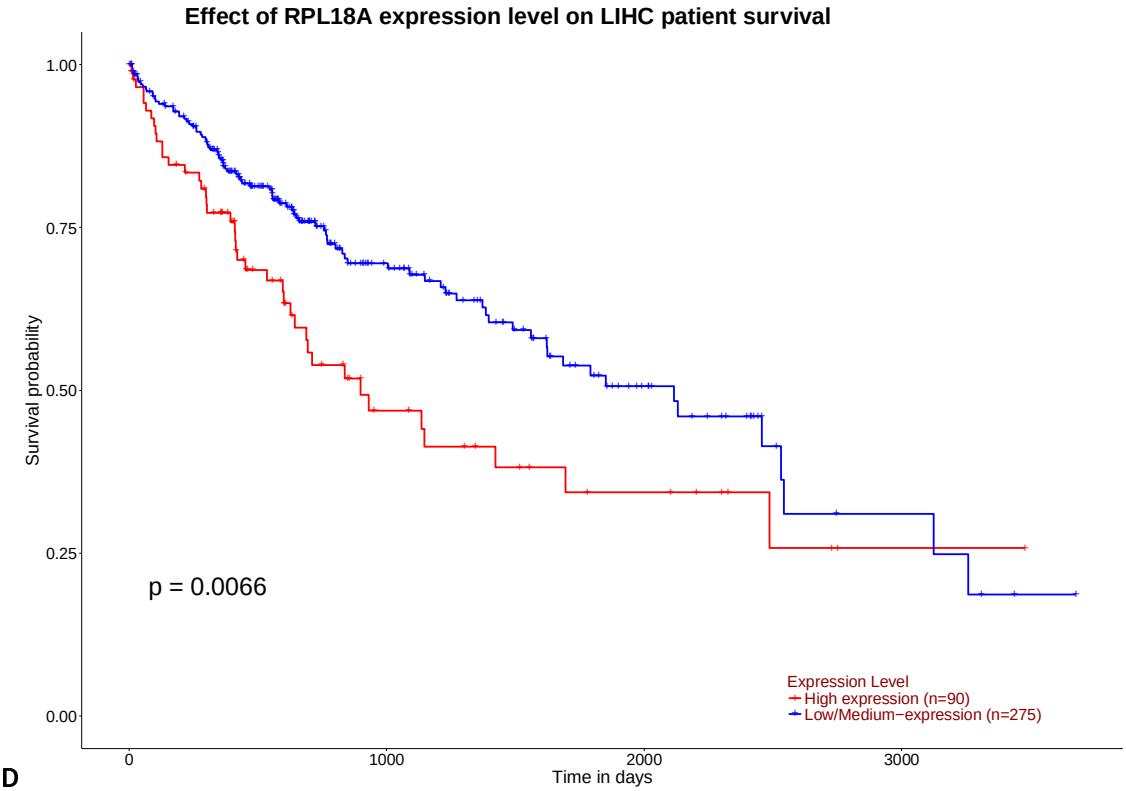
Effect of RPL18A expression level on LIHC patient survival
Survival probability
1.00
0.75
0.50
0.25
0.00
p = 0.0066
Expression Level
High expression (n=90)
Low/Medium−expression (n=275)
0
1000
2000
3000
Time in days

D

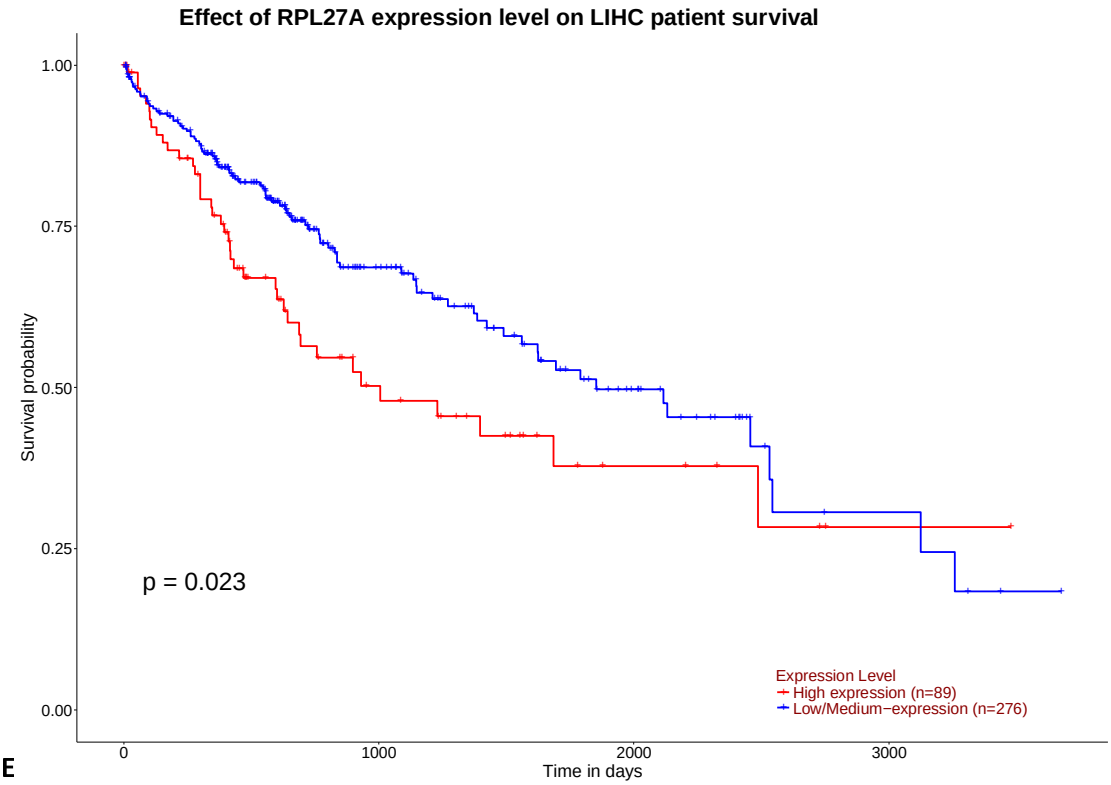
Effect of RPL27A expression level on LIHC patient survival
Survival probability
1.00
0.75
0.50
0.25
0.00
p = 0.023
Expression Level
High expression (n=89)
Low/Medium−expression (n=276)
0
1000
2000
3000
Time in days

E

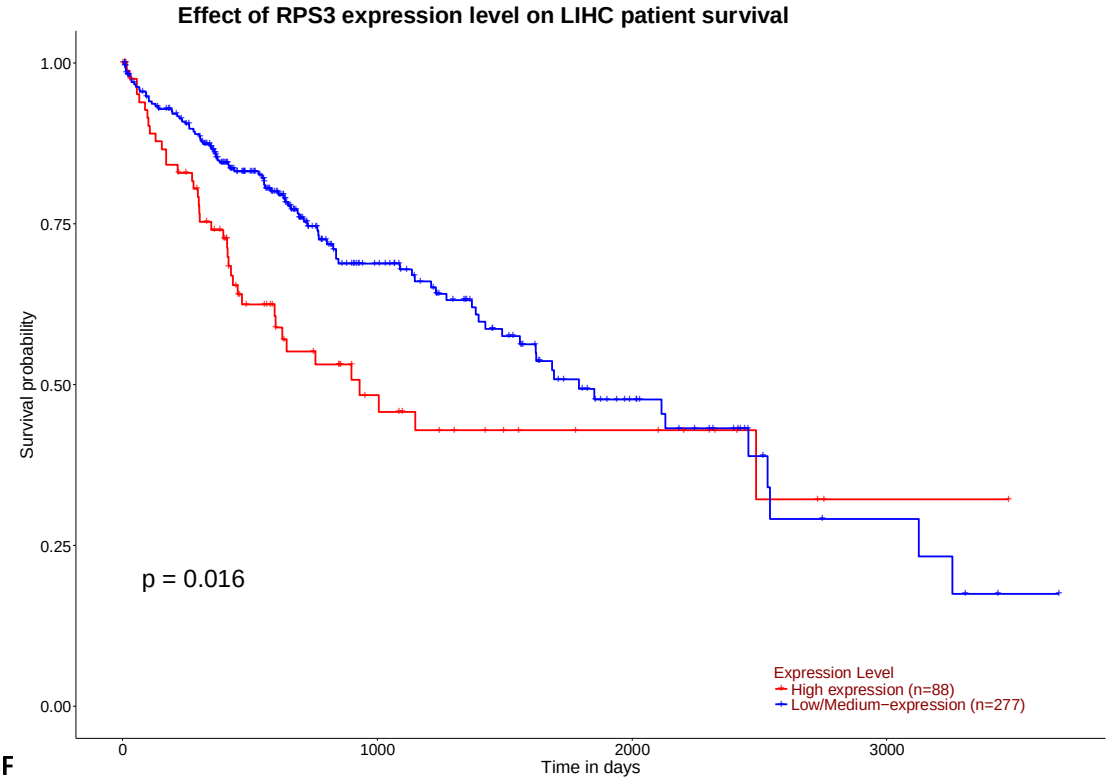
Effect of RPS3 expression level on LIHC patient survival
Survival probability
1.00
0.75
0.50
0.25
0.00
p = 0.016
Expression Level
High expression (n=88)
Low/Medium−expression (n=277)
0
1000
2000
3000
Time in days

F

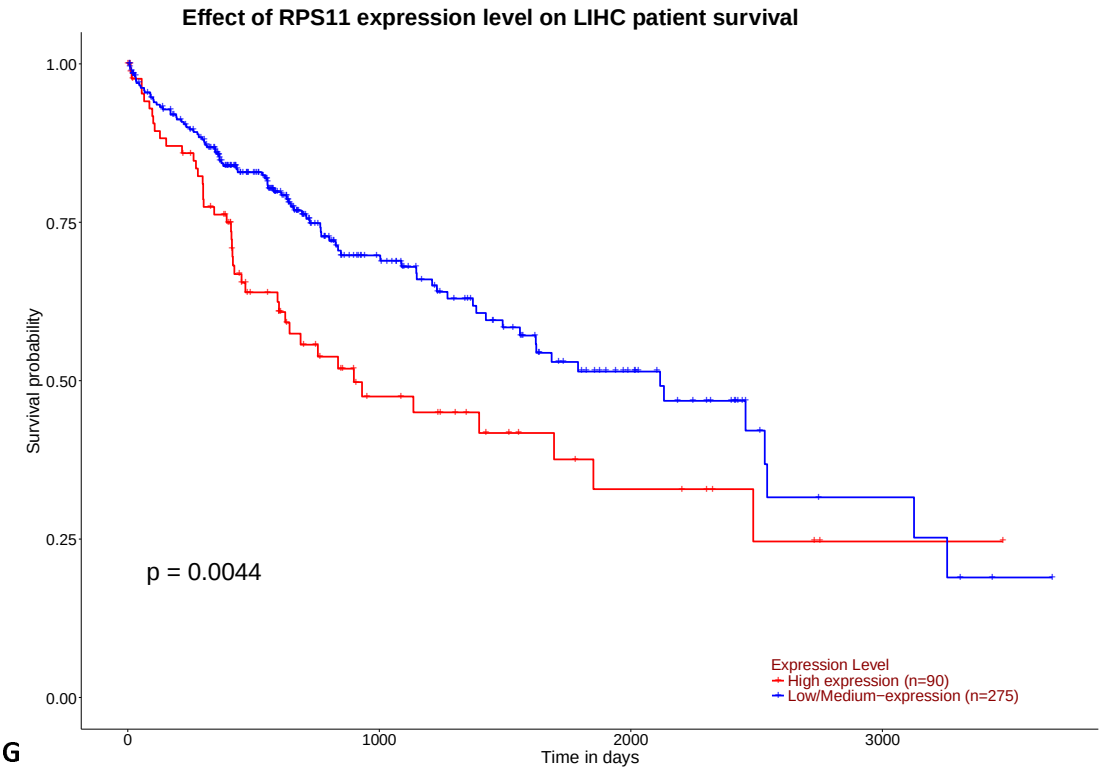

G

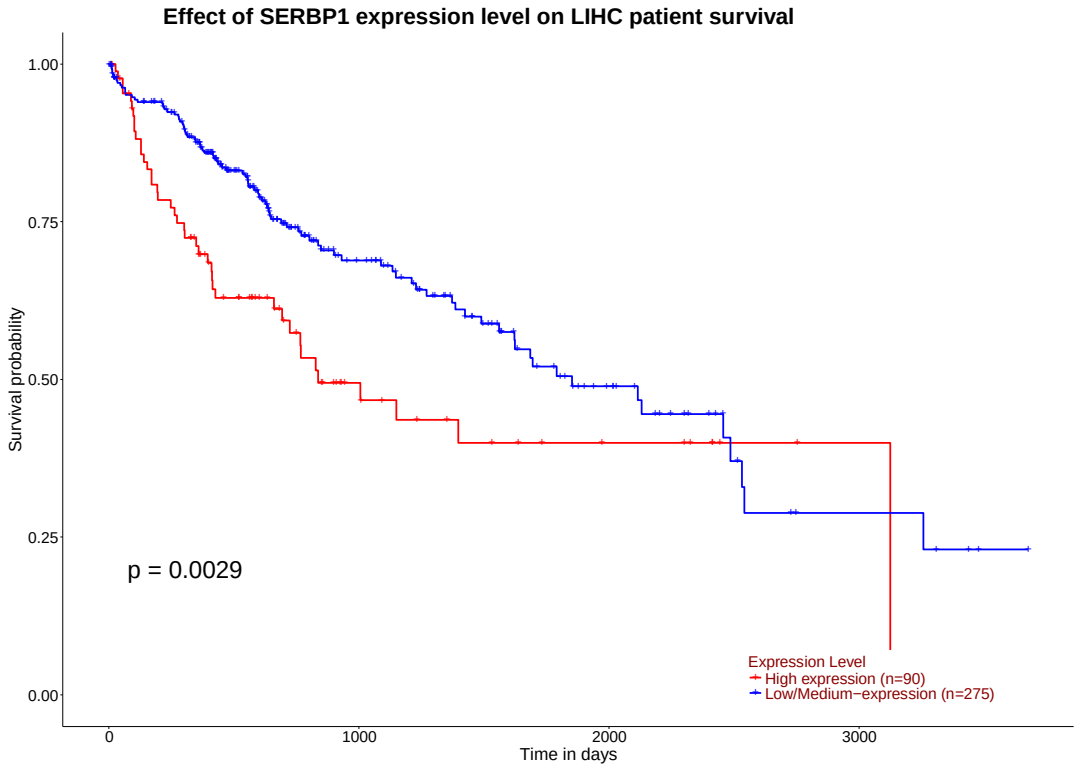

H

Figure 10. Survival Analysis of Hub genes. Survival Curve of **A,** EEF2 **B,** NDUFA8 **C,** RPL7A **D,** RPL 18A **E,** RPL27A **F,** RPS3 **G,** RPS11 **H,** SERBP1.

375 **Discussion**

376 Hepatocellular carcinoma (HCC) is a heterogeneous disease influenced by various
377 factors, including its multi-stage progression and a male-to-female incidence ratio of 4:1
378 (Park et al., 2015), making it a leading cause of mortality among men worldwide. Given this
379 complexity, using a single-gender animal model for HCC research is insufficient. This study
380 aims to provide gender-specific proteomic data from DEN-induced HCC mouse models to
381 better understand the distinct molecular mechanisms driving HCC's etiology, prevalence,
382 and pathogenesis in males and females, and to identify gender-specific biomarkers and
383 treatment strategies. While proteomic studies of HCC are common, comparative analyses
384 between genders are rare. Recent findings suggest male rodents show greater susceptibility
385 to hepatocarcinogenesis, indicating that gender-related molecular mechanisms contribute to
386 HCC prevalence in males. However, the underlying reasons for gender disparities in HCC
387 incidence, survival, and prognosis remain unclear.

388 Rong et al. (2017) reported that not only do gender-dependent biological processes
389 occur in hepatic tumorigenesis but also gender-dependent molecular responses to
390 oncogenes occur in normal hepatocytes. The study showed that in male mice pathways
391 associated with signal transduction, transport, and metabolism were upregulated while
392 females exhibited mostly downregulated metabolic and antioxidant proteins. Consistent
393 with this, our study showed that DEN-treated female mice represent upregulated catabolic
394 and metabolic pathways whereas pathways for fatty acid, sulfur compound, acyl-CoA,
395 thioester, and ribonucleotide metabolism were downregulated in DEN-treated female mice.
396 In addition to affirming the findings of Rong et al. (2017), the present study also indicates
397 that pathways associated with metabolic and catabolic processes were downregulated in
398 DEN-treated male mice as opposed to the case of female mice whereas pathways associated
399 with translation, mRNA binding, ribosome structure and binding were upregulated in male
400 mice.

401 Zhang et al (2024) reported in their study that DEN and CCl4-induced HCC mouse
402 models show significant upregulation of the actin cytoskeleton which is linked to the
403 activation of hepatic stellate cells (HSCs), which contributes to liver injury and collagen-rich
404 extracellular matrix formation. Consistent with these findings we observed enrichment of
405 pathways associated with structural constituent of cytoskeleton and cortical cytoskeleton,
406 particularly pathways associated with actin filament and binding. This alteration in the actin
407 cytoskeleton is crucial in cancer processes, suggesting it as a potential therapeutic target for
408 HCC in females.

409 DEN-treated male mice clearly showed distinct expression patterns compared to
410 their female counterparts. Most of the hub proteins obtained from PPI networks belonged
411 to either RNA binding proteins or ribosomal proteins indicating post-transcriptional
412 modifications in expression. Ribosomal proteins (RPs) are a family of canonical RBPs. In
413 addition to playing central roles in ribosome biogenesis and protein synthesis, RPs are also

414 found to be involved in cell proliferation, apoptosis, invasion, and metastasis via a number of
415 mechanisms including transcription regulation, autophagy, phosphorylation and RNA-
416 binding function (Warner and McIntosh, 2009; Ebright et al., 2020; Pecoraro et al., 2021;
417 Ceci et al., 2021), and therefore participate in the occurrence and development of multiple
418 cancers types including HCC (Zhou et al., 2024; Zhang et al., 2022). Nevertheless, to date,
419 only a few HCC-related RBPs have been well characterized. In our study RBPs have been
420 found to be extensively differentially enriched across genders. Hub gene analysis of DEN-
421 induced HCC in male mice shows that Rpl4, Rpl7a, Rpl27a, Rps29, Rps3, Rpl3, Rpl13, Rpl18a,
422 and Rps11 were upregulated in DEN-treated male mice whereas Hub gene analysis of DEN-
423 treated female mice didn't show enrichment of ribosomal pathways. To our knowledge this
424 is the first report of DEN-induced, gender-biased, perturbations in ribosomal proteins.
425 However, these results need to be further validated through Western blot analysis.

426 RPS3 has been frequently reported to be upregulated in human HCC and is found to
427 be associated with aggressiveness and promotion of hepatocarcinogenesis. Knockdown of
428 RPS3 has been found to almost completely abolish HCC tumorigenesis both in vitro and in
429 vivo (Schäfer et al., 2006). Consistent with the previous reports, we also reported the
430 upregulation of RPS3 and its association with poor survival outcomes in DEN-treated male
431 mice. RPL3 also plays a ubiquitous role in regulating tumor phenotypes, many clusters of
432 tumors with down-regulated RPL3, including HCC, kidney clear cell cancer, and brain cancer,
433 possessed inferior survival (Dolezal et al., 2018). The present study showed that RPL3 was
434 significantly upregulated in hub gene analysis, but it was not found to be significantly
435 associated with survival outcomes. Overexpression of RPS 11 is associated with poor
436 prognosis in glioblastoma (Yong et al., 2015). We have also reported that the upregulation of
437 RPS 11 in the DEN-induced HCC model of male mice is associated with poor survival. The
438 role of RPS 11 has not yet been established clearly in human hepatocellular carcinoma,
439 hence this study makes RPS 11 a potential candidate for evaluating its potential as a
440 prognostic marker and a therapeutic target. This study also reports the upregulation of
441 RPL13 in Hub gene analysis of DEN-treated male mice which has been correlated with
442 gastrointestinal malignancies (Kobayashi et al., 2006) but has not yet been reported in liver
443 cancer so far. Immunohistochemical staining of eEF2 and peEF2(T56) showed that this
444 protein and its phosphorylation are highly significant prognostic markers for the overall
445 survival of HCC patients (Pott et al., 2017) which has been consistently replicated in the
446 survival analysis of DEN-treated male mice, in this study.

447 The Ndufc2, Ndufv3, Ndufa8, Ndufa7, Ndufa2, and Ndufs6 hub genes in DEN-treated
448 female mice belonged to the NADH dehydrogenase (ubiquinone) oxidoreductase complex.
449 These hub genes are six out of at least 41 subunits of mitochondrial respiratory chain
450 complex 1 which is the 1st and largest enzyme complex of the electron transport chain.
451 Ndufa8 is the only protein in DEN-treated female mice that showed an association with
452 patient survival. Higher levels of Ndufa8 were associated with poor survival. It has not been
453 previously reported to be involved in liver cancer. Liver cells are highly regenerative and

require high energy hence a higher number of mitochondria. Abnormalities in mitochondrial metabolism are known to be carcinogenic factors (Jin et al., 2020). The role of complex 1 subunits in liver cancer has scarcely been studied so far, hence our findings open new vistas of research for exploring female HCC in the context of mitochondrial metabolic disease.

This study was conducted with a limited number of experimental animals. Notably, the early loss of three male mice reduced the sample size in that group; however, this observation aligns with previously reported gender-based differences in survival, where male subjects exhibit poorer outcomes in hepatocellular carcinoma (HCC) models compared to females. Our survival analysis supports this trend, as five proteins were associated with the male cohort, whereas only one protein showed significant association in females. Although direct experimental validation of several novel proteins identified through bioinformatics approaches (e.g., via Western blotting or immunohistochemistry) was not feasible due to resource constraints, the proteomic findings remained internally consistent and were further substantiated through literature-based validation.

Conclusion

We concluded that DEN-induced male and female mouse models for hepatocellular carcinoma exhibit distinct molecular signatures, thereby following different pathological and prognostic courses in clinical settings. The divergent groups of proteins associated with poor survival—ribosomal (RPS3, RPS 11) and RNA binding proteins (RPL7A, RPL 18A, RPL27A) in males, and mitochondrial complex I protein (NDUFA8) in females—can be further investigated as potential gender-specific prognostic markers and therapeutic targets. Developing gender-specific therapeutic regimens may open new prospects in the management of liver cancer, particularly in HCC.

Ethics Approval and Consent to Participate

All animal protocols were in accordance with ARRIVE guidelines and were approved by the ethical committee for research of International Islamic University Islamabad, Pakistan. The methods of this study were informed to all the authors and were conducted in accordance with relevant guidelines and regulations.

Data Availability Statement

Data is provided within the manuscript or supplementary files

Acknowledgments

We are grateful to the Pakistan Science Foundation for partially funding this research via PSF grant# 733. We are thankful to Molecular Oncology Research Lab for serving as a base camp for this project. We also appreciate Dr. Ikramullah for allowing us to use the animal house facility at the Center for Interdisciplinary Research in Basic Science (CIRBS), International Islamic University Islamabad. The study was supported by the VILLUM Center for Bio

analytical Sciences at University of Southern Denmark and by PRO-MS, Danish National Mass Spectrometry Platform for Functional Proteomics.

References

1. Bastide A, & David, A. (2018). The ribosome, (slow) beating heart of cancer (stem) cell. Oncogenesis, 7(4), 34. https://doi.org/10.1038/s41389-018-0044-8
2. Ceci, M., Fazi, F., & Romano, N. (2021). The role of RNA-binding and ribosomal proteins as specific RNA translation regulators in cellular differentiation and carcinogenesis. Biocchimica et biophysica acta. Molecular basis of disease, 1867(4), 166046. https://doi.org/10.1016/j.bbadis.2020.166046
3. Corley, M., Burns, M. C., & Yeo, G. W. (2020). How RNA-Binding Proteins Interact with RNA: Molecules and Mechanisms. Molecular cell, 78(1), 9–29. https://doi.org/10 https://doi.org/10.1016/j.bbamcr.2008.10.017
4. Kim, Y., Kim, H. D., & Kim, J. (2013). Cytoplasmic ribosomal protein S3 (rpS3) plays a pivotal role in mitochondrial DNA damage surveillance. Biochimica et biophysica acta, 1833(12), 2943–2952. https://doi.org/10.1016/j.bbamcr.2013.07.015
5. Kobayashi, T., Sasaki, Y., Oshima, Y., Yamamoto, H., Mita, H., Suzuki, H., Toyota, M., Tokino, T., Itoh, F., Imai, K., & Shinomura, Y. (2006). Activation of the ribosomal protein L13 gene in human gastrointestinal cancer. International journal of molecular medicine, 18(1), 161–170.
6. Kool, M., Koster, J., Bunt, J., Hasselt, N. E., Lakeman, A., van Sluis, P., Troost, D., Meeteren, N. S., Caron, H. N., Cloos, J., Mrsić, A., Ylstra, B., Grajkowska, W., Hartmann, W., Pietsch, T., Ellison, D., Clifford, S. C., & Versteeg, R. (2008). Integrated genomics identifies five medulloblastoma subtypes with distinct genetic profiles, pathway signatures and clinicopathological features. PloS one, 3(8), e3088. https://doi.org/10.1371/journal.pone.0003088
7. Liu, S., Li, B., Liang, Q., Liu, A., Qu, L., & Yang, J. (2020). Classification and function of RNA-protein interactions. Wiley interdisciplinary reviews. RNA, 11(6), e1601. https://doi.org/10.1002/wrna.1601
8. Pecoraro, A., Pagano, M., Russo, G., & Russo, A. (2021). Ribosome Biogenesis and Cancer: Overview on Ribosomal Proteins. International journal of molecular sciences, 22(11), 5496. https://doi.org/10.3390/ijms22115496
9. Pott, L. L., Hagemann, S., Reis, H., Lorenz, K., Bracht, T., Herold, T., Skryabin, B. V., Megger, D. A., Kälsch, J., Weber, F., Sitek, B., & Baba, H. A. (2017). Eukaryotic elongation factor 2 is a prognostic marker and its kinase a potential therapeutic target in HCC. *Oncotarget*, *8*(7), 11950–11962. https://doi.org/10.18632/oncotarget.14447
10. Rong, Z., Fan, T., Li, H., Li, J., Wang, K., Wang, X., Dong, J., Chen, J., Wang, F., Wang, J., & Wang, A. (2017). Differential Proteomic Analysis of Gender-dependent Hepatic Tumorigenesis in Hras12V Transgenic Mice. Molecular & cellular proteomics: MCP, 16(8), 1475–1490. https://doi.org/10.1074/mcp.M116.065474

11. Russo, A., Saide, A., Cagliani, R., Cantile, M., Botti, G., & Russo, G. (2016). rpL3 promotes the apoptosis of p53 mutated lung cancer cells by down-regulating CBS and NFκB upon 5-FU treatment. Scientific reports, 6, 38369. https://doi.org/10.1038/srep38369
12. Russo, A., Saide, A., Smaldone, S., Faraonio, R., & Russo, G. (2017). Role of uL3 in Multidrug Resistance in p53-Mutated Lung Cancer Cells. International journal of molecular sciences, 18(3), 547. https://doi.org/10.3390/ijms18030547
13. Schäfer, T., Maco, B., Petfalski, E., Tollervey, D., Böttcher, B., Aebi, U., & Hurt, E. (2006). Hrr25-dependent phosphorylation state regulates organization of the pre-40S subunit. Nature, 441(7093), 651–655. https://doi.org/10.1038/nature04840
14. Warner, J. R., & McIntosh, K. B. (2009). How common are extraribosomal functions of ribosomal proteins?. Molecular cell, 34(1), 3–11. https://doi.org/10.1016/j.molcel.2009.03.006
15. Wier, E. M., Neighoff, J., Sun, X., Fu, K., & Wan, F. (2012). Identification of an N-terminal truncation of the NF-κB p65 subunit that specifically modulates ribosomal protein S3-dependent NF-κB gene expression. The Journal of biological chemistry, 287(51), 43019–43029. https://doi.org/10.1074/jbc.M112.388694
16. Wu, Y., Meng, X., Huang, C., & Li, J. (2015). Emerging role of silent information regulator 1 (SIRT1) in hepatocellular carcinoma: a potential therapeutic target. Tumour biology : the journal of the International Society for Oncodevelopmental Biology and Medicine, 36(6), 4063–4074. https://doi.org/10.1007/s13277-015-3488-x
17. Yadavilli, S., Mayo, L. D., Higgins, M., Lain, S., Hegde, V., & Deutsch, W. A. (2009). Ribosomal protein S3: A multi-functional protein that interacts with both p53 and MDM2 through its KH domain. DNA repair, 8(10), 1215–1224. https://doi.org/10.1016/j.dnarep.2009.07.003
18. Yong, W. H., Shabihkhani, M., Telesca, D., Yang, S., Tso, J. L., Menjivar, J. C., Wei, B., Lucey, G. M., Mareninov, S., Chen, Z., Liau, L. M., Lai, A., Nelson, S. F., Cloughesy, T. F., & Tso, C. L. (2015). Ribosomal Proteins RPS11 and RPS20, Two Stress-Response Markers of Glioblastoma Stem Cells, Are Novel Predictors of Poor Prognosis in Glioblastoma Patients. PloS one, 10(10), e0141334. https://doi.org/10.1371/journal.pone.0141334
19. Zhang, K., Barry, A. E., Lamm, R., Patel, K., Schafer, M., & Dang, H. (2022). The role of RNA binding proteins in hepatocellular carcinoma. Advanced drug delivery reviews, 182, 114114. https://doi.org/10.1016/j.addr.2022.114114
20. Zhang, Q., Liu, Y., Ren, L., Li, J., Lin, W., Lou, L., Wang, M., Li, C., & Jiang, Y. (2024). Proteomic analysis of DEN and CCl4-induced hepatocellular carcinoma mouse model. Scientific Reports, 14(1), 8013. https://doi.org/10.1038/s41598-024-58587-6
21. Zhou, X., Liao, W. J., Liao, J. M., Liao, P., & Lu, H. (2015). Ribosomal proteins: functions beyond the ribosome. Journal of molecular cell biology, 7(2), 92–104. https://doi.org/10.1093/jmcb/mjv014

571 22. Zhou, Y. J., Yang, M. L., He, X., Gu, H. Y., Ren, J. H., Cheng, S. T., Fu, Z., Zhang, Z. Z., &
572 Chen, J. (2024). RNA-binding protein RPS7 promotes hepatocellular carcinoma
573 progression via LOXL2-dependent activation of ITGB1/FAK/SRC signaling. Journal of
574 experimental & clinical cancer research: CR, 43(1), 45.
575 https://doi.org/10.1186/s13046-023-02929-1

Table 1: List of Significantly Downregulated Proteins in Treated Female Mice

Protein IDs	Protein names	Unique peptides	Gene names
P62702	40S ribosomal protein S4, X isoform	16	Rps4x
Q9CRB3	5-hydroxyisourate hydrolase	9	Urah
Q9D1R9	60S ribosomal protein L34	8	Rpl34
Q8VCW8	Acyl-CoA synthetase family member 2, mitochondrial	31	Acsf2
Q8BGQ7	Alanine--tRNA ligase, cytoplasmic	33	Aars
P00329	Alcohol dehydrogenase 1	32	Adh1
Q8VC28	Aldo-keto reductase family 1 member C13	3	Akr1c13
P17182	Alpha-enolase	50	Eno1
B1AU25	Apoptosis-inducing factor 1, mitochondrial	27	Aifm1
Q3V117	ATP-citrate synthase	65	Acly
Q8CGC7	Bifunctional glutamate/proline--tRNA ligase;Glutamate--tRNA ligase;Proline--tRNA ligase	37	Eprs
Q8C196	Carbamoyl-phosphate synthase [ammonia], mitochondrial	177	Cps1
Q8VCT4	Carboxylesterase 1D	37	Ces1d
Q9CZU6	Citrate synthase, mitochondrial;Citrate synthase	22	Cs
P01027	Complement C3;Complement C3 beta chain;C3-beta-c;Complement C3 alpha chain;C3a anaphylatoxin;Acylation stimulating protein;Complement C3b alpha chain;Complement C3c alpha chain fragment 1;Complement C3dg fragment;Complement C3g fragment;Complement C3d fragment;Complement C3f fragment;Complement C3c alpha chain fragment 2	65	C3
P01029	Complement C4-B;Complement C4 beta chain;Complement C4 alpha chain;C4a anaphylatoxin;Complement C4 gamma chain	25	C4b
P00405	Cytochrome c oxidase subunit 2	6	Mtco2
P00186	Cytochrome P450 1A2	17	Cyp1a2
P15392	Cytochrome P450 2A4	9	Cyp2a4
P28271	Cytoplasmic aconitate hydratase	47	Aco1
Q99L04	Dehydrogenase/reductase SDR family member 1	18	Dhrs1
Q9D2G2	Dihydrolipoyllysine-residue succinyltransferase component of 2-oxoglutarate dehydrogenase complex, mitochondrial	19	Dlst
P50285	Dimethylaniline monooxygenase [N-oxide-forming] 1	19	Fmo1
Q8JZQ9	Eukaryotic translation initiation factor 3 subunit B	13	Eif3b
P19096	Fatty acid synthase;[Acyl-carrier-protein] S-	126	Fasn

	acetyltransferase;[Acyl-carrier-protein] S-malonyltransferase;3-oxoacyl-[acyl-carrier-protein] synthase;3-oxoacyl-[acyl-carrier-protein] reductase;3-hydroxyacyl-[acyl-carrier-protein] dehydratase;Enoyl-[acyl-carrier-protein] reductase;Oleoyl-[acyl-carrier-protein] hydrolase		
Q3UER8	Fibrinogen gamma chain	16	Fgg
A0A0A0MQF6	Glyceraldehyde-3-phosphate dehydrogenase	29	Gapdh
B1ASZ3	Glycerol kinase	13	Gyk;Gk
O35969	Guanidinoacetate N-methyltransferase	6	Gamt
P54869	Hydroxymethylglutaryl-CoA synthase, mitochondrial	41	Hmgcs2
P40936	Indolethylamine N-methyltransferase	18	Inmt
Q61703	Inter-alpha-trypsin inhibitor heavy chain H2	6	Itih2
Q9CXF0	Kynureninase	14	Kynu
P06151	L-lactate dehydrogenase A chain;L-lactate dehydrogenase	30	Ldha
Q8JZR0	Long-chain-fatty-acid--CoA ligase 5	21	Acsl5
A0A1Y7VJZ2	Maleylacetoacetate isomerase	15	Gstz1
O08601	Microsomal triglyceride transfer protein large subunit	34	Mttp
Q91X91	Nicotinate-nucleotide pyrophosphorylase [carboxylating]	10	Qprt
E9PZF0	Nucleoside diphosphate kinase;Nucleoside diphosphate kinase B	7	Gm20390
P24369	Peptidyl-prolyl cis-trans isomerase B	19	Ppib
P35700	Peroxiredoxin-1	31	Prdx1
Q9QXD1	Peroxisomal acyl-coenzyme A oxidase 2	27	Acox2
Q9DBM2	Peroxisomal bifunctional enzyme;Enoyl-CoA hydratase/3,2-trans-enoyl-CoA isomerase;3-hydroxyacyl-CoA dehydrogenase	52	Ehhadh
Q60866	Phosphotriesterase-related protein	16	Pter
P20918	Plasminogen;Plasmin heavy chain A;Activation peptide;Angiostatin;Plasmin heavy chain A, short form;Plasmin light chain B	24	Plg
Q9DCQ2	Putative L-aspartate dehydrogenase	17	Aspdh
P61027	Ras-related protein Rab-10	3	Rab10
P62821	Ras-related protein Rab-1A	6	Rab1A
O88451	Retinol dehydrogenase 7	13	Rdh7
Q9R0P3	S-formylglutathione hydrolase	12	Esd
P80316	T-complex protein 1 subunit epsilon	17	Cct5
Q9D0R2	Threonine--tRNA ligase, cytoplasmic	25	Tars
P61089	Ubiquitin-conjugating enzyme E2 N	8	Ube2n
Q3UEL5	Urocanate hydratase	33	Uroc1

Table 2: List of Significantly Upregulated Proteins in Treated Female Mice

Protein IDs	Protein names	Unique peptides	Gene names
Q99JT9	1,2-dihydroxy-3-keto-5-methylthiopentene dioxygenase	11	Adi1
Q64433	10 kDa heat shock protein, mitochondrial	29	Hspe1
P68510	14-3-3 protein eta	8	Ywhah
P58871	182 kDa tankyrase-1-binding protein	20	Tnks1bp1
Q9CQX8	28S ribosomal protein S36, mitochondrial	4	Mrps36
Q283N4	2-oxo-4-hydroxy-4-carboxy-5-ureidoimidazoline decarboxylase	15	Urad
P62858	40S ribosomal protein S28	14	Rps28
L7N466	5-formyltetrahydrofolate cyclo-ligase	1	Mthfsl
P63038	60 kDa heat shock protein, mitochondrial	86	Hspd1
Q9EST5	Acidic leucine-rich nuclear phosphoprotein 32 family member B	7	Anp32b
Q99JY9	Actin-related protein 3	21	Actr3
P55264	Adenosine kinase	13	Adk
P46656	Adrenodoxin	10	Fdx1
P57780	Alpha-actinin-4	42	Actn4
P09813	Apolipoprotein A-II	5	Apoa2
Q9D3D9	ATP synthase subunit delta	7	Atp5d
P56382	ATP synthase subunit epsilon	9	Atp5e
P97450	ATP synthase-coupling factor 6	13	Atp5j
E9PV44	ATPase inhibitor, mitochondrial	15	Atpif1
E9PZ16	Basement membrane-specific heparan sulfate proteoglycan core protein	29	Hspg2
P26231	Catenin alpha-1	19	Ctnna1
Q61490	CD166 antigen	13	Alcam
D3YVV1	Cell cycle control protein 50A	7	Tmem30a
P23198	Chromobox protein homolog 3	8	Cbx3
P45591	Cofilin-2	9	Cfl2
Q8R3Q6	Coiled-coil domain-containing protein 58	12	Ccdc58
Q9WUM4	Coronin-1C	12	Coro1c
Q9CPZ8	COX assembly mitochondrial protein homolog	4	Cmc1
Q9DCT8	Cysteine-rich protein 2	10	Crip2
P56395	Cytochrome b5	20	Cyb5a
Q9D855	Cytochrome b-c1 complex subunit 7	19	Uqcrb
Q8BGD8	Cytochrome c oxidase assembly factor 6 homolog	3	Coa6
Q921H9	Cytochrome c oxidase assembly factor 7	9	Coa7

P56391	Cytochrome c oxidase subunit 6B1	14	Cox6b1
O88487	Cytoplasmic dynein 1 intermediate chain 2	7	Dync1i2
Q91XC8	Death-associated protein 1	9	Dap
P97821	Dipeptidyl peptidase 1 exclusion domain chain	5	Ctsc
A2A5S3	Double-stranded RNA-binding protein Staufen homolog 1	8	Stau1
Q62418	Drebrin-like protein	15	Dbnl
O70251	Elongation factor 1-beta	20	Eef1b
Q9D172	ES1 protein homolog, mitochondrial	24	D10Jhu81e
Q9Z1D1	Eukaryotic translation initiation factor 3 subunit G	11	Eif3g
Q8BGD9	Eukaryotic translation initiation factor 4B	30	Eif4b
P59325	Eukaryotic translation initiation factor 5	15	Eif5
Q3U0V1	Far upstream element-binding protein 2	24	Khsrp
P09528	Ferritin heavy chain	20	Fth1
P29391	Ferritin light chain 1	6	Ftl1
A0A494BAI5	Ferrochelatase	10	Fech
Q3U9N4	Granulins	16	Grn
Q99LP6	GrpE protein homolog 1	20	Grpel1
Q9R257	Heme-binding protein 1	14	Hebp1
Q5EBP8	Heterogeneous nuclear ribonucleoprotein	11	Hnrnpa1
Q60668	Heterogeneous nuclear ribonucleoprotein D0	16	Hnrnpd
B2M1R6	Heterogeneous nuclear ribonucleoprotein K	32	Hnrnpk
Q9D0E1	Heterogeneous nuclear ribonucleoprotein M	40	Hnrnpm
Q8VEK3	Heterogeneous nuclear ribonucleoprotein U	27	Hnrnpu
Q9Z204	Heterogeneous nuclear ribonucleoproteins C1/C2	19	Hnrnpc
A0A0J9YUZ4	High mobility group protein B1	21	Hmgb1
P17095	High mobility group protein HMG-I/HMG-Y	2	Hmga1
A0A0R4J039	Histidine-rich glycoprotein	13	Hrg
P15864	Histone H1.2	14	Hist1h1c
P43277	Histone H1.3	3	Hist1h1d
Q60972	Histone-binding protein RBBP4	4	Rbbp4
Q9CQW9	Interferon-induced transmembrane protein 3	2	Ifitm3
Q61029	Lamina-associated polypeptide 2	12	Tmpo
Q9ERG0	LIM domain and actin-binding protein 1	16	Lima1
O09159	Lysosomal alpha-mannosidase	10	Man2b1
A0A1W2P711	Melanoma inhibitory activity protein 2	24	Mia2
A0A0R4J2D3;	Melanoma inhibitory activity protein 3	36	Mia3
O55022	Membrane-associated progesterone receptor component 1	19	Pgrmc1
Q9EQ20	Methylmalonate-semialdehyde dehydrogenase [acylating]	45	Aldh6a1
P27546	Microtubule-associated protein 4	9	Map4
A0A0R4J0N9	Microtubule-associated tumor suppressor 1 homolog	5	Mtus1
Q9WVA2	Mitochondrial import inner membrane translocase	9	Timm8a1

	subunit Tim8 A		
Q9WV98	Mitochondrial import inner membrane translocase subunit Tim9	5	Timm9
P62774	Myotrophin	7	Mtpn
Q9JHL1	Na(+)/H(+) exchange regulatory cofactor NHE-RF2;Na(+)/H(+) exchange regulatory cofactor NHE-RF	6	Slc9a3r2
Q9JIL4	Na(+)/H(+) exchange regulatory cofactor NHE-RF3	31	Pdzk1
Q8C5H8	NAD kinase 2, mitochondrial	3	Nadk2
Q9CQ75	NADH dehydrogenase [ubiquinone] 1 alpha subcomplex subunit 2	11	Ndufa2
Q9Z1P6	NADH dehydrogenase [ubiquinone] 1 alpha subcomplex subunit 7	14	Ndufa7
Q9DCJ5	NADH dehydrogenase [ubiquinone] 1 alpha subcomplex subunit 8	12	Ndufa8
Q9CQ54	NADH dehydrogenase [ubiquinone] 1 subunit C2	5	Ndufc2
P52503	NADH dehydrogenase [ubiquinone] iron-sulfur protein 6, mitochondrial	8	Ndufs6
Q02819	Nucleobindin-1	41	Nucb1
P09405	Nucleolin	58	Ncl
Q61937	Nucleophosmin	27	Npm1
Q8CHP5	Partner of Y14 and mago	9	Wibg
P17742	Peptidyl-prolyl cis-trans isomerase A	22	Ppia
Q99KR7	Peptidyl-prolyl cis-trans isomerase F	15	Ppif
Q9D1M7	Peptidyl-prolyl cis-trans isomerase FKBP11	4	Fkbp11
P45878	Peptidyl-prolyl cis-trans isomerase FKBP2	15	Fkbp2
Q9QXS1	Plectin	30	Plec
O70591	Prefoldin subunit 2	9	Pfdn2
Q03958	Prefoldin subunit 6	11	Pfdn6
P49935	Pro-cathepsin H	12	Ctsh
D3Z7C6	Prostaglandin E synthase 3	7	Ptges3
Q9QXT0	Protein canopy homolog 2	17	Cnpy2
Q9DAU1	Protein canopy homolog 3	7	Cnpy3
Q9CR98	Protein FAM136A	16	Fam136a
Q80WJ7	Protein LYRIC	11	Mtdh
Q91XF0	Pyridoxine-5-phosphate oxidase	19	Pnpo
P97855	Ras GTPase-activating protein-binding protein 1	8	G3bp1
Q99PT1	Rho GDP-dissociation inhibitor 1	12	Arhgdia
P52760	Ribonuclease UK114	17	Hrsp12
Q9D1J3	SAP domain-containing ribonucleoprotein	8	Sarnp
E9Q3V6	Septin-2	10	2-Sep
Q9EP89	Serine beta-lactamase-like protein LACTB	5	Lactb
Q91VW3	SH3 domain-binding glutamic acid-rich-like protein 3	7	Sh3bgrl3
Q9CYR0	Single-stranded DNA-binding protein	8	Ssbp1
Q3V2H3	Sorting nexin-12	8	Snx12
Q9D8U8	Sorting nexin-5	15	Snx5

P16546	Spectrin alpha chain	1	Sptan1	
Q62261	Spectrin beta chain	26	Sptbn1	
Q60598	Src substrate cortactin	14	Cttn	
Q9CQA3	Succinate dehydrogenase [ubiquinone] iron-sulfur subunit	20	Sdhb	
Q9D5V6	Synapse-associated protein 1	4	Syap1	
Q9CQU0	Thioredoxin domain-containing protein 12	11	Txndc12	
Q9CQM5	Thioredoxin domain-containing protein 17	5	Txndc17	
Q569Z6	Thyroid hormone receptor-associated protein 3	17	Thrap3	
P39447	Tight junction protein ZO-1	14	Tjp1	
P83940	Transcription elongation factor B polypeptide 1	6	Tceb1	
Q64152	Transcription factor BTF3	7	Btf3	
Q9CQH7	Transcription factor BTF3 homolog 4	7	Btf3l4	
Q9QUI0	Transforming protein RhoA	13	Rhoa	
P17751	Triosephosphate isomerase	32	Tpi1	
P21107	Tropomyosin alpha-3 chain	4	Tpm3	
P48428	Tubulin-specific chaperone A	12	Tbca	
Q9CYZ2	Tumor protein D54	13	Tpd52l2	
Q922Y1	UBX domain-containing protein 1	12	Ubxn1	
Q9DCS2	UPF0585 protein C16orf13 homolog	10		
Q8BH80	Vesicle-associated membrane protein-associated protein B	16	Vapb	
P20152	Vimentin	38	Vim	
A0A2I3BRB9		2		
D3Z2H9		18	Tpm3-rs7	
E9QA16		0		Cald1
F8WID5		1	Tpm1	
Q3U422		9	Ndufv3	

Table 3: List of Significantly Upregulated Proteins in Treated Male Mice

Protein IDs	Protein names	Unique peptides	Gene names
Q9CQV8	14-3-3 protein beta/alpha;14-3-3 protein beta/alpha, N-terminally processed	10	Ywhab
P62281	40S ribosomal protein S11	12	Rps11
P62274	40S ribosomal protein S29	6	Rps29
P62908	40S ribosomal protein S3	13	Rps3
P47963	60S ribosomal protein L13	21	Rpl13
P62717	60S ribosomal protein L18a	11	Rpl18a
P14115	60S ribosomal protein L27a	9	Rpl27a

P27659	60S ribosomal protein L3	18	Rpl3
Q9D8E6	60S ribosomal protein L4	35	Rpl4
P12970	60S ribosomal protein L7a	25	Rpl7a
Q8BGA8	Acyl-coenzyme A synthetase ACSM5, mitochondrial	25	Acsm5
G3X982	Aldehyde oxidase 3	28	Aox3
Q8VC28	Aldo-keto reductase family 1 member C13	3	Akr1c13
P22599	Alpha-1-antitrypsin 1-2	6	Serpina1b
O09174	Alpha-methylacyl-CoA racemase	23	Amacr
Q06185;Q8BTB6	ATP synthase subunit e, mitochondrial	14	Atp5i
O88696	ATP-dependent Clp protease proteolytic subunit, mitochondrial	11	Clpp
A0A3Q4L347	Cysteine dioxygenase type 1	5	Cdo1
Q9DBE0	Cysteine sulfinic acid decarboxylase	22	Csad
P99028	Cytochrome b-c1 complex subunit 6, mitochondrial	10	Uqcrh
Q62425	Cytochrome c oxidase subunit NDUFA4	9	Ndufa4
Q9D2G2	Dihydrolipoyllysine-residue succinyltransferase component of 2-oxoglutarate dehydrogenase complex, mitochondrial	19	Dlst
Q9EQF5	Dihydropyrimidinase	32	Dpys
Q9D172	ES1 protein homolog, mitochondrial	24	D10Jhu81e
A0A494BB95	Eukaryotic translation initiation factor 1A, X-chromosomal;Eukaryotic translation initiation factor 1A	5	Eif1ax;Eif1a;Gm8300; Gm2016;Gm2056; Gm6803;Gm2035;Gm5039
Q8R1B4	Eukaryotic translation initiation factor 3 subunit C	14	Eif3c
Q6NZJ6	Eukaryotic translation initiation factor 4 gamma 1	30	Eif4g1
P05064	Fructose-bisphosphate aldolase A;Fructose-bisphosphate aldolase	23	Aldoa;Aldoart1
P97807	Fumarate hydratase, mitochondrial	30	Fh
P19157	Glutathione S-transferase P 1	22	Gstp1
O35969	Guanidinoacetate N-methyltransferase	6	Gamt
Q9D0E1	Heterogeneous nuclear ribonucleoprotein M	40	Hnrnpm
Q8VEK3	Heterogeneous nuclear ribonucleoprotein U	27	Hnrnpu
P10922	Histone H1.0;Histone H1.0, N-terminally processed	23	H1f0
P15864	Histone H1.2	14	Hist1h1c
P62806	Histone H4	15	Hist1h4a
Q9CXF0	Kynureninase	14	Kynu
Q61029	Lamina-associated polypeptide 2, isoforms beta/delta/epsilon/gamma;Lamina-	12	Tmpo

	associated polypeptide 2, isoforms alpha/zeta		
P21619	Lamin-B2	17	Lmnb2
Q61792	LIM and SH3 domain protein 1	18	Lasp1
A2CEL1	Major urinary protein 1	0	Mup1;Mup15
P11589	Major urinary protein 2	2	Mup2
Q3KQQ2	Major urinary protein 3	7	Mup3
Q60605	Myosin light polypeptide 6	12	Myl6
Q60817	Nascent polypeptide-associated complex subunit alpha;Nascent polypeptide-associated complex subunit alpha, muscle-specific form	7	Naca
P29595	NEDD8	5	Nedd8
P09405	Nucleolin	58	Ncl
Q9CY58	Plasminogen activator inhibitor 1 RNA-binding protein	17	Serbp1
P48678	Prelamin-A/C;Lamin-A/C	41	Lmna
Q6TCG2	Progestin and adipoQ receptor family member 9	5	Paqr9
O35955	Proteasome subunit beta type-10	5	Psmb10
Q8QZR3	Pyrethroid hydrolase Ces2a	16	Ces2a
Q9Z1Z2	Serine-threonine kinase receptor-associated protein	9	Strap
Q64442	Sorbitol dehydrogenase	35	Sord
Q9Z2I8	Succinyl-CoA ligase [GDP-forming] subunit beta, mitochondrial	29	Suclg2
P21107	Tropomyosin alpha-3 chain	4	Tpm3
A0A0R4J0I1		6	
A0A0R4J135		3	Selenbp2
A2BIN1		0	Mup10
D3Z158		10	Qars
D3Z2H9		18	Tpm3-rs7

Table 4: List of Significantly Downregulated Proteins in Treated Male Mice

Protein IDs	Protein names	Unique peptides	Gene names
P62334	26S protease regulatory subunit 10B	19	Psmc6
O88685	26S protease regulatory subunit 6A	20	Psmc3
P26516	26S proteasome non-ATPase regulatory subunit 7	8	Psmd7
Q283N4	2-oxo-4-hydroxy-4-carboxy-5-	15	Urad

	ureidoimidazoline decarboxylase		
A2AFQ2	3-hydroxyacyl-CoA dehydrogenase type-2	16	Hsd17b10
Q99JY9	Actin-related protein 3	21	Actr3
A0A0R4J0I6	Acyl-CoA dehydrogenase family member 11	17	Acad11
J3QN31	Adenylosuccinate synthetase isozyme 1	5	Adssl1
P51881	ADP/ATP translocase 2;ADP/ATP translocase 2, N-terminally processed	28	Slc25a5
Q9CZS1	Aldehyde dehydrogenase X, mitochondrial	27	Aldh1b1
P17182	Alpha-enolase	50	Eno1
Q01339	Beta-2-glycoprotein 1	19	Apoh
P48758	Carbonyl reductase [NADPH] 1	26	Cbr1
O88587	Catechol O-methyltransferase	16	Comt
P10605	Cathepsin B;Cathepsin B light chain;Cathepsin B heavy chain	11	Ctsb
O55029	Coatomer subunit beta	9	Copb2
Q61129	Complement factor I;Complement factor I heavy chain;Complement factor I light chain	12	Cfi
Q9WUM3	Coronin-1B	16	Coro1b
Q9D855	Cytochrome b-c1 complex subunit 7	19	Uqcrb
P19783	Cytochrome c oxidase subunit 4 isoform 1, mitochondrial	19	Cox4i1
P12787	Cytochrome c oxidase subunit 5A, mitochondrial	10	Cox5a
P56391	Cytochrome c oxidase subunit 6B1	14	Cox6b1
Q9D0M3	Cytochrome c1, heme protein, mitochondrial	8	Cyc1
Q9R0P5	Destrin	11	Dstn
P63037	DnaJ homolog subfamily A member 1	8	Dnaja1
Q8BL66	Early endosome antigen 1	42	Eea1
P58252	Elongation factor 2	57	Eef2
Q9WUR2	Enoyl-CoA delta isomerase 2, mitochondrial	14	Eci2
Q9D7J9	Enoyl-CoA hydratase domain-containing protein 3, mitochondrial	8	Echdc3
Q05816	Fatty acid-binding protein, epidermal	24	Fabp5
E9PV24	Fibrinogen alpha chain;Fibrinopeptide A;Fibrinogen alpha chain	43	Fga
Q9Z1Z0	General vesicular transport factor	18	Uso1

	p115		
Q00612	Glucose-6-phosphate 1-dehydrogenase X;Glucose-6-phosphate 1-dehydrogenase	12	G6pdx
Q9DCM2	Glutathione S-transferase kappa 1	14	Gstk1
Q64471	Glutathione S-transferase theta-1	16	Gstt1
Q61133	Glutathione S-transferase theta-2	7	Gstt2
Q64521	Glycerol-3-phosphate dehydrogenase, mitochondrial;Glycerol-3-phosphate dehydrogenase	26	Gpd2
Q99LP6	GrpE protein homolog 1, mitochondrial	20	Grpel1
Q9WTP7	GTP:AMP phosphotransferase AK3, mitochondrial	28	Ak3
P63017	Heat shock cognate 71 kDa protein	52	Hspa8
P38060	Hydroxymethylglutaryl-CoA lyase, mitochondrial	22	Hmgcl
P40936	Indolethylamine N-methyltransferase	18	Inmt
A0A1L1STE6	Isocitrate dehydrogenase [NAD] subunit alpha, mitochondrial	14	Idh3a
O88844	Isocitrate dehydrogenase [NADP] cytoplasmic	50	Idh1
Q9Z2I0	LETM1 and EF-hand domain-containing protein 1, mitochondrial	19	Letm1
Q8VBT2	L-serine dehydratase/L-threonine deaminase	11	Sds
P70699	Lysosomal alpha-glucosidase	9	Gaa
Q6ZQI3	Malectin	4	Mlec
Q3ULD5	Methylcrotonoyl-CoA carboxylase beta chain, mitochondrial	19	Mccc2
Q9EQ20	Methylmalonate-semialdehyde dehydrogenase [acylating], mitochondrial	45	Aldh6a1
Q8CAQ8	MICOS complex subunit Mic60	10	Immt
P62075	Mitochondrial import inner membrane translocase subunit Tim13	9	Timm13
Q9D6Y7	Mitochondrial peptide methionine sulfoxide reductase	17	Msra
Q9JIL4	Na(+)/H(+) exchange regulatory cofactor NHE-RF3	31	Pdzk1
Q8C5H8	NAD kinase 2, mitochondrial	3	Nadk2
Q9CPP6	NADH dehydrogenase [ubiquinone] 1 alpha subcomplex subunit 5	8	Ndufa5
Q9JMD3	PCTP-like protein	11	Stard10

Q8CI51	PDZ and LIM domain protein 5	7	Pdlim5
P43883	Perilipin-2	25	Plin2
O70591	Prefoldin subunit 2	9	Pfdn2
Q91ZA3	Propionyl-CoA carboxylase alpha chain, mitochondrial	35	Pcca
Q9WVE8	Protein kinase C and casein kinase substrate in neurons protein 2	16	Pacsin2
Q3UM45	Protein phosphatase 1 regulatory subunit 7	11	Ppp1r7
P36993	Protein phosphatase 1B	1	Ppm1b
P21981	Protein-glutamine gamma-glutamyltransferase 2	20	Tgm2
E9Q509	Pyruvate kinase;Pyruvate kinase PKLR	53	Pklr
Q64374	Regucalcin	40	Rgn
Q9JLI6	Selenocysteine lyase	12	Scly
P50431	Serine hydroxymethyltransferase, cytosolic;Serine hydroxymethyltransferase	30	Shmt1
Q76MZ3	Serine/threonine-protein phosphatase 2A 65 kDa regulatory subunit A alpha isoform	17	Ppp2r1a
Q99JR1	Sideroflexin-1	9	Sfxn1
Q9D8U8	Sorting nexin-5	15	Snx5
Q9CQA3	Succinate dehydrogenase [ubiquinone] iron-sulfur subunit, mitochondrial	20	Sdhb
E9QNL5	Sulfotransferase	5	Sult1a1
P42932	T-complex protein 1 subunit theta	23	Cct8
Q9CQM5	Thioredoxin domain-containing protein 17	5	Txndc17
Q62264	Thyroid hormone-inducible hepatic protein	8	Thrsp
Q9CYZ2	Tumor protein D54	13	Tpd52l2
Q8K1Z0	Ubiquinone biosynthesis protein COQ9, mitochondrial	13	Coq9
P50544	Very long-chain specific acyl-CoA dehydrogenase, mitochondrial	31	Acadvl
Q8BH80	Vesicle-associated membrane protein-associated protein B	16	Vapb
Q8CC88	von Willebrand factor A domain-containing protein 8	10	Vwa8
A0A075B5N7		3	Igkv6-13
E9Q5K4		14	Cyp2c44
Q99L20		14	Gstt3